

Supporting Information

for

Aggregation-induced phosphorescence enhancement in deep-red and near-infrared emissive iridium(III) complexes for solution-processable OLEDs

Hae Un Kim,^{a,‡} Ho Jin Jang,^{b,‡} Wanuk Choi,^c Sungjin Park,^a Taiho Park^{a*}, Jun Yeob Lee,^{b*} and K. S. Bejoymohandas^{a*}

^aDepartment of Chemical Engineering, Pohang University of Science and Technology, 77 Cheongam-Ro, Nam-Gu, Pohang, Gyeongbuk 37673, Korea

^bSchool of Chemical Engineering, Sungkyunkwan University 2066, Seobu-ro, Jangan-gu, Seobu-ro, Suwon, Gyeonggi, 16419, Korea

^cDivision of Environmental Science and Engineering, Pohang University of Science and Technology, 77 Cheongam-Ro, Nam-Gu, Pohang, Gyeongbuk 37673, Korea

*E-mail: bejoymohan@postech.ac.kr, leej17@skku.edu, taihopark@postech.ac.kr

Contents

Scheme S1 Synthesis of **L2** and General synthetic pathways toward the iridium(III) complexes **Ir1-Ir4**.

Figure S1 $^1\text{H-NMR}$ spectrum of 2-(benzo[b]thiophen-2-yl)-4-phenylquinoline (**L2**).

Figure S2 $^{13}\text{C-NMR}$ spectrum of 2-(benzo[b]thiophen-2-yl)-4-phenylquinoline (**L2**).

Figure S3 ESI-Mass spectrum of 2-(benzo[b]thiophen-2-yl)-4-phenylquinoline (**L2**).

Figure S4 $^1\text{H-NMR}$ spectrum of bis[2-(benzo[b]thiophen-2-yl)-4-phenylquinolate]iridium(III) (picolate): $(\text{btpq})_2\text{Ir}(\text{pic})$ (**Ir2**).

Figure S5 $^{13}\text{C-NMR}$ spectrum of bis[2-(benzo[b]thiophen-2-yl)-4-phenylquinolate]iridium(III) (picolate): $(\text{btpq})_2\text{Ir}(\text{pic})$ (**Ir2**).

Figure S6 MALDI TOF MASS spectrum of bis[2-(benzo[b]thiophen-2-yl)-4-phenylquinolate]iridium(III) (picolate): $(\text{btpq})_2\text{Ir}(\text{pic})$ (**Ir2**).

Figure S7 $^1\text{H-NMR}$ spectrum of bis[ethyl 2-(benzo[b]thiophen-2-yl)quinoline-4-carboxylate]iridium(III) (picolate): $(\text{btecq})_2\text{Ir}(\text{pic})$ (**Ir3**).

Figure S8 $^{13}\text{CNMR}$ spectrum of bis[ethyl 2-(benzo[b]thiophen-2-yl)quinoline-4-carboxylate]iridium(III) (picolate): $(\text{btecq})_2\text{Ir}(\text{pic})$ (**Ir3**).

Figure S9 MALDI TOF MASS spectrum of bis[ethyl 2-(benzo[b]thiophen-2-yl)quinoline-4-carboxylate] iridium(III) (picolate): $(\text{btecq})_2\text{Ir}(\text{pic})$ (**Ir3**).

Figure S10 $^1\text{H-NMR}$ spectrum of bis[2-(benzo[b]thiophen-2-yl)-4-(trifluoromethyl)quinoline]iridium(III) (picolate): $(\text{bttmq})_2\text{Ir}(\text{pic})$ (**Ir4**).

Figure S11 $^{13}\text{C-NMR}$ spectrum of bis[2-(benzo[b]thiophen-2-yl)-4-(trifluoromethyl)quinoline]iridium(III) (picolate): $(\text{bttmq})_2\text{Ir}(\text{pic})$ (**Ir4**).

Figure S12 $^{19}\text{F-NMR}$ spectrum of bis[2-(benzo[b]thiophen-2-yl)-4-(trifluoromethyl)quinoline]iridium(III) (picolate): $(\text{bttmq})_2\text{Ir}(\text{pic})$ (**Ir4**).

Figure S13 MALDI TOF MASS spectrum of bis[2-(benzo[b]thiophen-2-yl)-4-(trifluoromethyl)quinoline] iridium(III) (picolate): $(\text{bttmq})_2\text{Ir}(\text{pic})$ (**Ir4**).

Figure S14 Thermogravimetric curves for complex **Ir1 Ir4** under nitrogen atmosphere.

Figure S15 Differential scanning calorimetric curves for complex **Ir1 Ir4** under nitrogen atmosphere.

Figure S16 Optimized geometries of **Ir1-Ir4** at the PBE1PBE/6-31G* level.

Figure S17 Optimized geometries of **Ir1-Ir4** exhibits dipole moment at the PBE1PBE/6-31G* level.

Figure S18 Cyclic voltammograms of redox processes of complexes **Ir1-Ir4**

Figure S19. Comparison of experimental (red line) and Calculated absorption spectra (TD-DFT) for **Ir1-Ir4**.

Figure S20. Comparison of experimental FT-IR Spectrum with the IR intensity obtained from the optimized triplet and singlet geometries of **Ir1** and **Ir2**.

Figure S21 Comparison of experimental FT-IR Spectrum with the IR intensity obtained from the optimized triplet and singlet geometries of **Ir3** and **Ir4**.

Figure S22 Comparison of lifetime decay profiles of complex **Ir1 Ir4** in degassed dichloromethane.

Figure S23 Emission spectrum, variation of peak intensity ratio and peak wavelength change of **Ir1** and **Ir2** in acetone–hexane mixtures with increasing hexane fractions at room temperature.

Figure S24 Two-dimensional and three-dimensional AFM images of emissive layers of RD1-1, RD1-2, RD2-1 and RD2-2.

Figure S25 Electroluminescence spectra from RD1-1, RD1-2, RD2-1 and RD2-2 PhOLEDs as a function of applied voltages during operation.

Table S1 Selected Bond Lengths for Complexes **Ir1-Ir4**.

Table S2 Selected Bond Angles for **Ir1** and **Ir2**.

Table S3 Selected Bond Angles for **Ir3** and **Ir4**.

Table S4. Crystallographic and refinement data for complexes **Ir2-Ir4**.

Table S5. Selected bond distances, bond angles and dihedral angles from the optimized ground (S_0) and triplet state (T_1) geometry for the complexes **Ir1-Ir4** together with the experimental values.

Table S6. Optimized geometries, HOMO-2, HOMO-1, HOMO, LUMO, LUMO+1 and LUMO+2 contour plots of **Ir1-Ir4** at the PBE1PBE/6-31G* level.

Table S7 Calculated energy levels of the HOMO, HOMO-1, HOMO-2, LUMO, LUMO+1, and LUMO+2 and percentage of contribution of iridium metal (Ir), benzothiophenequinolate derivatives and picolate (pic) ligands.

Table S8 Calculated Absorption of **Ir1-Ir4** in CH_2Cl_2 Media at TD-B3LYP Level together with Experimental Values.

EXPERIMENTAL SECTION

Materials and physical measurements. A 400 MHz Bruker NMR spectrometer was used to record the ^1H , ^{19}F and ^{13}C NMR spectra of the iridium(III) complex in CDCl_3 solution. The chemical shifts (δ) of the signals are given in ppm and referenced to the internal standard tetramethylsilane $[\text{Si}(\text{CH}_3)_4]$. The signals splitting is abbreviated as follows: s = singlet; d = doublet; t = triplet; dd = doublet of doublets; dq = doublet of quintets; td = triplet of doublets; m = multiplet. Coupling constants (J) are given in Hertz (Hz). Magnesium sulphate (anhydrous), sodium carbonate, sodium hydroxide, tetrakis(triphenylphosphine) palladium(0), $\text{IrCl}_3 \cdot x(\text{H}_2\text{O})$, 4-trifluoromethyl-2 (1H) -quinolinone, 2-hydroxyquinoline-4-carboxylic acid, POCl_3 , thionyl chloride, 2-bromoquinoline, 2-chloro-4-methylquinoline, benzo[b]thiophene-2-boronic acid and 4,4,4-trifluoro-1-(2-thienyl)-1,3-butanedione were employed in the synthesis of the iridium(III) complex (**Ir1-Ir4**). These chemicals were purchased from Sigma Aldrich and were used without any further purification. The synthesis of the iridium dimer complex $[(\text{C}^{\wedge}\text{N})_2\text{Ir}(\mu\text{-Cl})]_2$ was carried out by a standard procedure proposed by Watts and co-workers,¹ using $\text{IrCl}_3 \cdot x(\text{H}_2\text{O})$ and cyclometalating ligands (**L1**, **L3** and **L4**) in a mixture of 2-ethoxyethanol and water. The dimers from **L1**, **L3** and **L4** were synthesized following same procedure from our earlier reports. The cyclometalating ligands and precursor compounds, **L1a**, **L3a**, **L4a**, **L1**, **L3** and **L4**, were synthesized by the method in our previous paper.² Thin-layer chromatography (TLC) was used to monitor the reaction progress (silica gel 60 F254, Merck Co.) and the spots were observed under UV light at 254 and 365 nm. Silica column chromatography was performed using silica gel (230–400 mesh, Merck Co.). The dry solvents are purified using J.C. Metyer solvent drying system. All other reagents are of analytical grade and used as received from Aldrich, Alfa Aesar and Samchun chemicals unless otherwise specified.

Synthesis of 2-(benzo[b]thiophen-2-yl)-4-phenylquinoline [btpq] (L2). 2-acetylbenzothiophene (1 g, 4.2 mmol), 2-aminobenzophenone (0.91 g, 4.6 mmol), diphenylphosphate (DPP, 1.27 g, 5.1 mmol) and m-cresol (5 ml) were stirred for 20 min. under nitrogen flush at room temperature and stirred for 24 h at 140 °C. Then 10% trimethylamine/ethanol was added and precipitate was formed. Vacuum filtration was used to collect the precipitate. The precipitate obtained has been separated by filtration by washing with 10% triethylamine in ethanol: dried and took NMR and it was clear product. The soluble part was done column as per procedure and cannot isolate anything (messy) wrong procedure. Lack

of clarity. The filtrate was eluted using silica gel. A solid was obtained after vacuum concentration. Recrystallization was done twice from chloroform and hexane to give product in 82% yield. ^1H NMR (400 MHz, Chloroform-*d*) δ 8.22 (dd, $J = 8.6, 1.2$ Hz, 1H), 7.99 (s, 1H), 7.96 – 7.84 (m, 3H), 7.82 (dt, $J = 6.7, 2.9$ Hz, 1H), 7.73 (m, 1H), 7.61 – 7.50 (m, 5H), 7.47 (m, 1H), 7.43 – 7.32 (m, 2H). ^{13}C NMR (151 MHz, CDCl_3) δ 151.86, 149.03, 148.70, 145.60, 141.23, 140.51, 138.13, 129.91, 129.77, 129.56, 128.67, 128.57, 126.58, 126.20, 125.74, 125.32, 124.52, 124.31, 122.64, 122.49, 118.10. (ESI-Mass) [$\text{C}_{23}\text{H}_{15}\text{NS}$]: calcd, $m/z = 337.09$; found, $m/z = 338.17$.

Synthesis of iridium(III) dimer complex $[(\text{L}2)_2\text{Ir}(\mu\text{-Cl})]_2$. $\text{IrCl}_3 \cdot x\text{H}_2\text{O}$ (180 mg, 0.66 mmol) and 2-(benzo[*b*]thiophen-2-yl)-4-phenylquinoline (**L2**) (350 mg, 1.33 mmol) were dissolved in 20 mL of 2-ethoxyethanol and water (3:1) mixture and refluxed at 140 °C for 24 h. After cooling the reaction mixture, the addition of 20 mL of H_2O gave a dark red precipitate that was filtered and washed with diethyl ether. The crude product was used for the next reaction without further purification (yield: 85%).

General synthesis procedure for complexes Ir1 – Ir4. A mixture of one equivalent of the corresponding dimer, 2.6 equivalents of picolinic acid and 11 equivalents of sodium carbonate were stirred overnight in a 3:1 mixture of dichloromethane and ethanol (40 mL) at 60 °C under argon atmosphere. The solvent was removed by evaporation under reduced pressure. The crude product obtained was poured into water and extracted with ethyl acetate (3×50 mL). The combined organic layer was dried over Na_2SO_4 . The solvent was removed under reduced pressure to give a crude residue. The crude product was purified by using silica gel column chromatography with CH_2Cl_2 : methanol in 9:1 ratio as eluent, giving the desired complex as dark red powder (for **Ir1** and **Ir2**) or black powder (for **Ir3** and **Ir4**) All purified samples were recrystallized and vacuum dried before conducting all analysis

Spectral data of bis[2-(benzo[*b*]thiophen-2-yl)-4-phenylquinolate]iridium(III) (picolate): $(\text{btpq})_2\text{Ir}(\text{pic}) = \text{Ir2}$. Yield: 76%. Anal. Calcd (%) for $\text{C}_{52}\text{H}_{32}\text{IrN}_3\text{O}_2\text{S}_2$: C, 63.27; H, 3.27; N, 4.26; S, 6.50, Found: C, 63.50; H, 3.07; N, 4.21; S, 6.32. ^1H NMR (400 MHz, Methylene Chloride-*d*₂) δ 8.49 (dd, $J = 8.9, 1.2$ Hz, 1H), 8.20 (dt, $J = 5.4, 1.2$ Hz, 1H), 7.89 (d, $J = 3.5$ Hz, 2H), 7.84 (m, 2H), 7.79 – 7.73 (m, 4H), 7.74 – 7.69 (m, 2H), 7.69 – 7.53 (m, 8H), 7.39 (m, 2H), 7.31 (m, 1H), 7.16 (m, 2H), 7.08 – 7.00 (m, 2H), 6.82 – 6.69 (m, 3H), 6.60 (m, 1H),

6.18 (d, $J = 8.0$ Hz, 1H). ^{13}C NMR (151 MHz, CD_2Cl_2) δ 171.23, 166.78, 165.62, 153.50, 152.46, 151.78, 151.60, 149.96, 148.99, 147.01, 146.94, 146.36, 142.96, 142.86, 140.18, 138.62, 138.25, 137.07, 131.33, 129.86, 129.75, 129.44, 129.11, 129.06, 128.73, 128.72, 127.76, 127.22, 127.16, 127.01, 126.40, 126.37, 126.26, 125.80, 125.66, 125.58, 125.27, 124.82, 124.62, 124.14, 123.68, 122.73, 122.67, 118.47, 117.66. (MALDI-TOF-MS) [$\text{C}_{52}\text{H}_{32}\text{IrN}_3\text{O}_2\text{S}_2$]: calcd, $m/z = 987.16$; found, $m/z = 987.2$ [M+].

Spectral data of bis[ethyl 2-(benzo[b]thiophen-2-yl)quinoline-4-carboxylate]iridium(III) (picolate): (btecq)₂Ir(pic) = Ir3. Yield: 70%. Anal. Calcd (%) for $\text{C}_{46}\text{H}_{32}\text{IrN}_3\text{O}_6\text{S}_2$: C, 56.43; H, 3.29; N, 4.29, S, 6.55, Found: C, 56.43; H, 3.29; N, 4.29, S, 6.55. ^1H NMR (400 MHz, Chloroform-*d*) δ 8.62 – 8.55 (m, 1H), 8.51 – 8.40 (m, 2H), 8.30 (d, $J = 4.4$ Hz, 2H), 8.05 (d, $J = 5.5$ Hz, 1H), 7.84 (d, $J = 8.1$ Hz, 1H), 7.74 (dd, $J = 13.0, 7.9$ Hz, 2H), 7.70 – 7.62 (m, 1H), 7.45 – 7.31 (m, 4H), 7.25 – 7.13 (m, 2H), 7.07 – 6.95 (m, 2H), 6.74 – 6.65 (m, 3H), 6.54 (t, $J = 7.8$ Hz, 1H), 6.05 (d, $J = 8.1$ Hz, 1H), 4.67 – 4.54 (m, 4H), 1.57 (t, $J = 2.2$ Hz, 6H). ^{13}C NMR (151 MHz, CDCl_3) δ 171.51, 167.21, 165.55, 165.49, 165.29, 155.26, 152.29, 152.11, 150.27, 149.08, 146.75, 146.64, 145.95, 143.11, 142.95, 140.35, 138.45, 138.43, 138.15, 138.10, 132.29, 129.61, 127.73, 127.54, 127.47, 127.15, 126.94, 126.84, 126.63, 125.91, 125.86, 125.84, 125.38, 124.57, 124.55, 123.89, 123.40, 122.75, 122.70, 122.36, 119.99, 118.29, 62.56, 62.38, 14.40, 14.34. (MALDI-TOF-MS) [$\text{C}_{46}\text{H}_{32}\text{IrN}_3\text{O}_6\text{S}_2$]: calcd, $m/z = 979.11$; found, $m/z = 979.16$ [M+].

Spectral data of bis[2-(benzo[b]thiophen-2-yl)-4-(trifluoromethyl)quinoline]iridium(III) (picolate): (bttmq)₂Ir(pic) = Ir4. Yield: 80%. Anal. Calcd (%) for $\text{C}_{42}\text{H}_{22}\text{F}_6\text{IrN}_3\text{O}_2\text{S}_2$: C, 51.95; H, 2.28; N, 4.33, S, 6.60, Found: C, 51.95; H, 2.28; N, 4.33, S, 6.60. ^1H NMR (400 MHz, Chloroform-*d*) δ 8.49 – 8.42 (m, 1H), 8.12 (d, $J = 7.7$ Hz, 2H), 8.04 (d, $J = 5.3$ Hz, 1H), 7.99 (d, $J = 8.5$ Hz, 1H), 7.93 (d, $J = 7.9$ Hz, 1H), 7.86 (d, $J = 8.0$ Hz, 1H), 7.81 – 7.77 (m, 1H), 7.75 – 7.65 (m, 3H), 7.56 – 7.37 (m, 4H), 7.31 – 7.16 (m, 2H), 7.09 – 6.94 (m, 2H), 6.80 – 6.72 (m, 2H), 6.70 (d, $J = 8.1$ Hz, 1H), 6.56 (ddd, $J = 8.2, 7.1, 1.1$ Hz, 1H), 6.00 (d, $J = 8.2$ Hz, 1H). ^{13}C NMR (151 MHz, CDCl_3) δ 171.44, 167.23, 165.61, 156.89, 153.74, 152.03, 150.19, 149.08, 146.58, 146.43, 145.95, 143.32, 143.18, 140.35, 138.68, 138.18, 137.13, 136.99, 136.92, 136.78, 132.85, 130.22, 127.95, 127.64, 127.52, 127.40, 127.34, 126.83, 126.37, 126.10, 125.77, 125.35, 124.81, 124.73, 124.04, 123.71, 122.92, 122.87, 121.89, 121.04, 120.07, 116.32, 116.28. ^{19}F NMR (471 MHz, CDCl_3) δ -61.40, -61.55. (MALDI-TOF-MS) [$\text{C}_{42}\text{H}_{22}\text{F}_6\text{IrN}_3\text{O}_2\text{S}_2$]: calcd, $m/z = 970.98$; found, $m/z = 971.08$ [M+].

Thermal analysis. Thermo-gravimetric analyses were performed on an TG/DTA Q500 (TA Instrument) heated from 30 to 800°C in flowing of nitrogen at the heating rate of 10 °C min⁻¹. Temperature at which a 5% weight loss occurred has been considered as the decomposition temperature (T_d). Differential scanning calorimetry was performed using a Perkin-Elmer Pyris DSC 4000 instrument in sealed aluminum pans under nitrogen flow at a heat/cooling rate of 5°C/min. The endothermic peak observed in the second heating cycle has been considered as the glass transition temperature (T_g).

Cyclic voltammetry. Cyclic voltammetry experiments were carried out with a PowerLab/AD instrument model system using three electrode cell assemblies. Platinum wires were used for counter electrodes, a silver wire was used as Ag/Ag⁺ quasi reference electrode and a platinum electrode was used as a working electrode. Measurements were carried out in dichloromethane solution with tetrabutylammonium hexafluorophosphate as supporting electrolyte at a scan rate of 100 mV/s. Concentrations of iridium(III) complex and supporting electrolyte were 5×10⁻³ and 0.2 M, respectively. The ferrocenium/ferrocene couple (FeCp₂⁺/FeCp₂⁰) was used as an internal reference. The energy level of FeCp₂⁺/FeCp₂⁰ was assumed at -4.8 eV to vacuum.³ All solutions for the electrochemical studies were deaerated with pre-purified argon gas prior to the measurements.

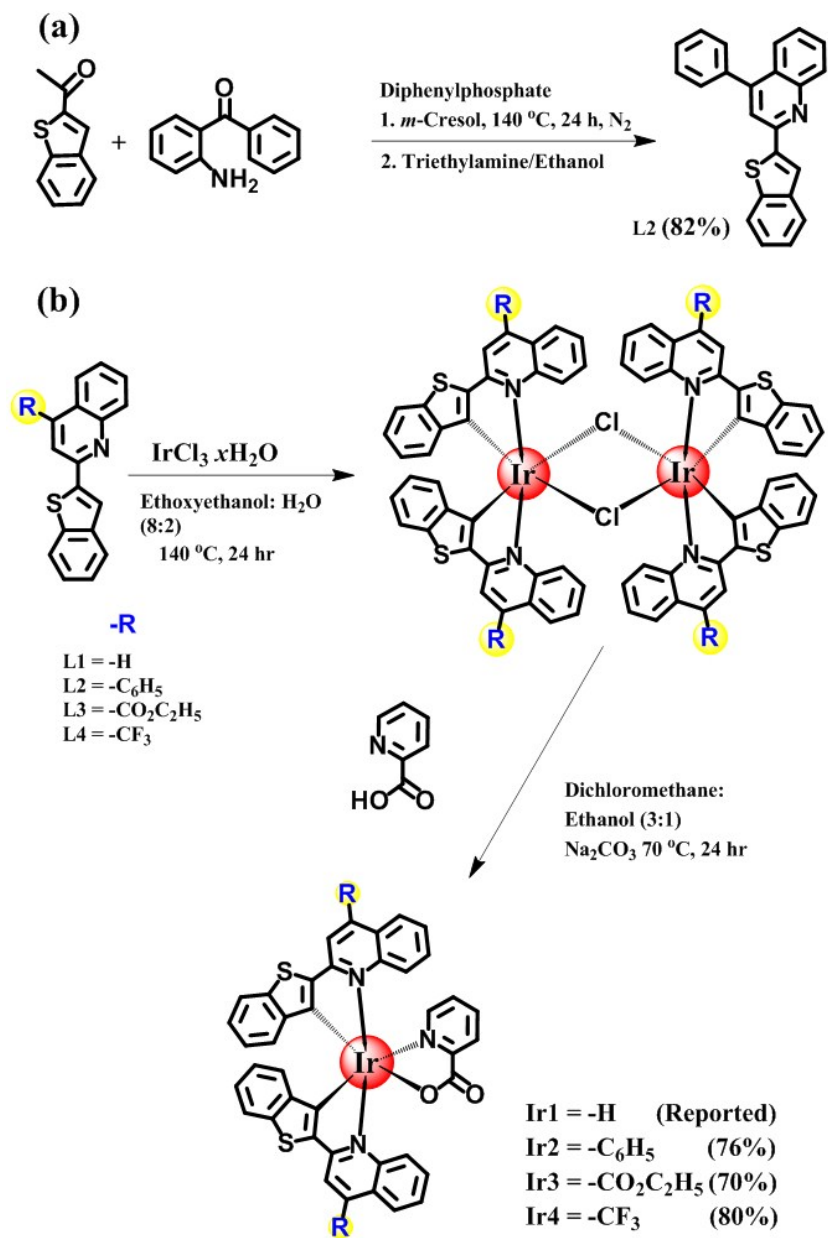
Computational methods. The geometrical structures of the singlet ground state (S_0) and the lowest lying triplet excited state (T_1) were optimized by using density functional theory (DFT) based on a method with Perdew-Burke-Ernzerhof (PBE0) hybrid functional with LANL2DZ basis set for the Iridium (Ir) atom and 6-31G* for the rest of the atoms. Frequency calculations were also executed at the same level of theory. The optimizations and the vibrational data confirmed that the structures were true minima on the potential energy surface because there were no imaginary frequencies. On the basis of the optimized ground and excited state geometry structures, the absorption spectral properties in dichloromethane media were calculated by time-dependent density functional theory (TD-DFT) approach with B3LYP/6-31G*. As solvent effects are known to play a crucial role in predicting the absorption and emission spectra, the same was incorporated in the TD-DFT calculations within the PCM framework. The Swizard program has been employed to evaluate the contribution of singly excited state configurations to each electronic transition.⁴ All calculations were carried out with Gaussian 16 package.⁵

Photophysical characterization. The electronic absorption spectrum of the complex was measured on a Mecasys Optizen Pop UV/vis spectrophotometer. The photoluminescence (PL) spectrum of the iridium(III) complex was recorded on a spectrofluorimeter (FP-6500, JASCO). Emission and excitation spectra were corrected for source intensity (lamp and grating) by standard correction curves. Phosphorescence lifetimes were measured using time correlated single photon counting (TCSPC) system (HAMAMATSU/C11367-31). The luminescence quantum efficiencies in the solution as well as film states were calculated by Quantaaurus-QY Absolute PL quantum yield spectrometer (C11347-11).

PhOLED device fabrication. The structure of device of **Ir2** was Indium tin oxide(ITO) (50nm) / poly(3,4-ethylenedioxythiophene) polystyrene sulfonate(PEDOT:PSS) (60nm) / Poly vinyl carbazole (PVK) (10nm) / 4,4'-di(9 H-carbazol-9-yl)biphenyl(CBP) : 1,3,5-tris(N-phenylbenzimidazole-2-yl)benzene (TPBi) : **Ir2** (40nm, 75:25:X%) / TPBi (45 nm) /LiF (1 nm) / Al (200 nm). In case of **Ir4**, the device structure was ITO (50nm) / PEDOT:PSS (60nm) / PVK (10nm)/ 4,4',4''-Tris(carbazol-9-yl)triphenylamine (TCTA) : 2,4,6-Tris[3-(diphenylphosphinyl)phenyl]-1,3,5-triazine (PO-T2T) : **Ir4** (30nm, 50 : 50, X%) / TPBi (45 nm) /LiF (1 nm) / Al (200 nm).

HTL and EML processed in solution process by spincoating. PVK solution which was 3mg/ml of chlorobenzene solution was spin-coated at 2000rpm for 30s, and annealed at 150°C for 30min. EML host for **Ir2** was mixed with CBP solution which was 10mg/ml of toluene solution and TPBi solution which was 10mg/ml of toluene solution in 75%:25% respectively. **Ir2** was dissolved in chloroform in 5mg/ml. EML host for **Ir4** was mixed with TCTA solution which was 7mg/ml of toluene solution and POT2T solution which was 7mg/ml of chlorobenzene solution in 50%:50% respectively. **Ir4** was dissolved in chloroform in 5mg/ml. Each dopant was doped in host for 10% and 15%. Mixed EML solution was spin-coated at 2000rpm for 30s, and annealed at 80°C for 20min.

ETL, and EIL were thermally evaporated under a high vacuum ($\sim 10^{-7}$ torr). ETL was TPBi and thermally deposited at 1 Å/s and LiF at 0.1Å/s. Al was deposited as cathode at 1Å/s under $\sim 10^{-6}$ torr. After deposition of cathode, devices were protected from oxygen and moisture by encapsulating with an encapsulation glass, CaO getter, and epoxy adhesive.



Scheme S1 Synthesis of **L2** and General synthetic pathways toward the iridium(III) complexes **Ir1-Ir4**.

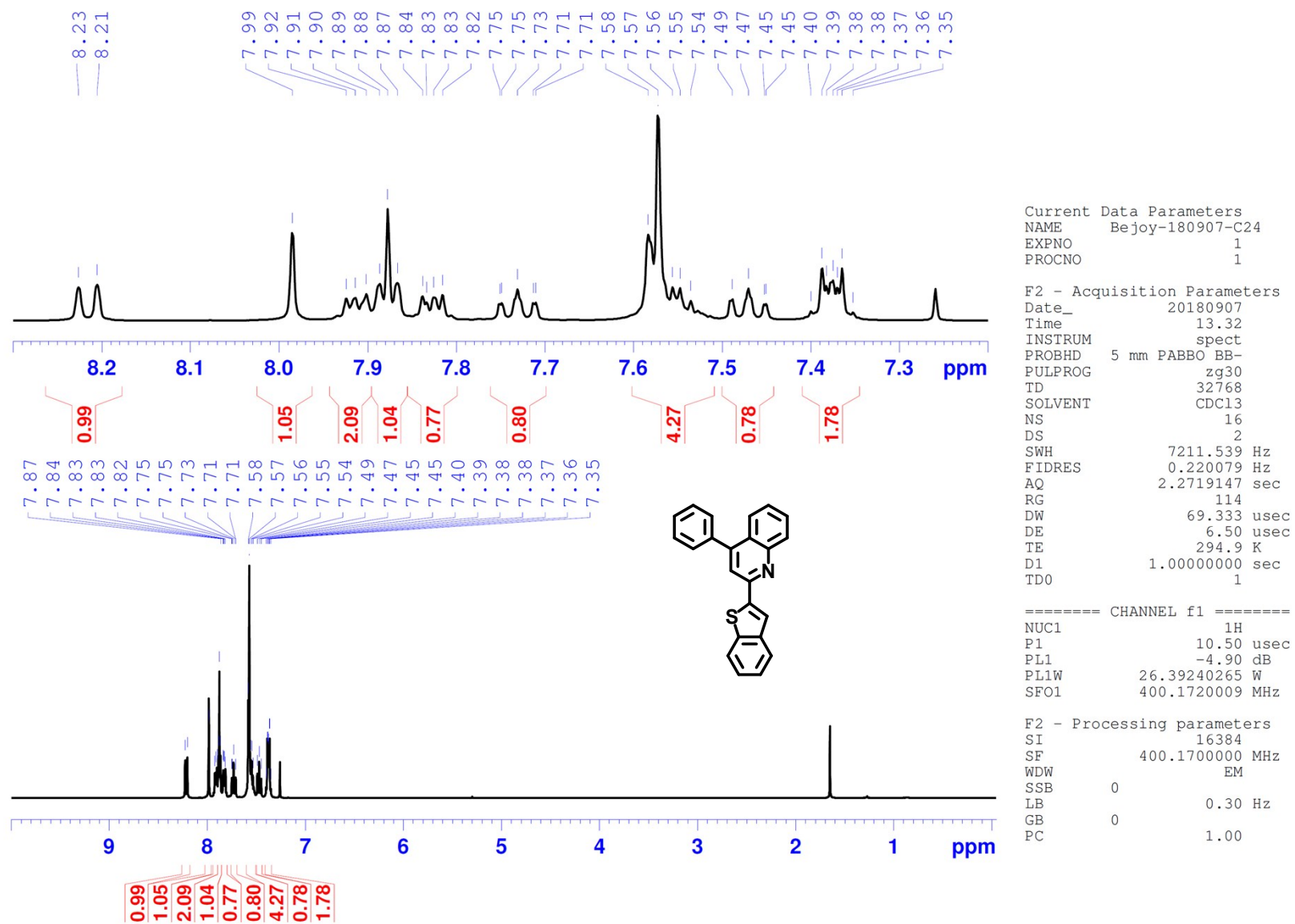


Figure S1 ¹H-NMR spectrum of 2-(benzo[b]thiophen-2-yl)-4-phenylquinoline (L2).

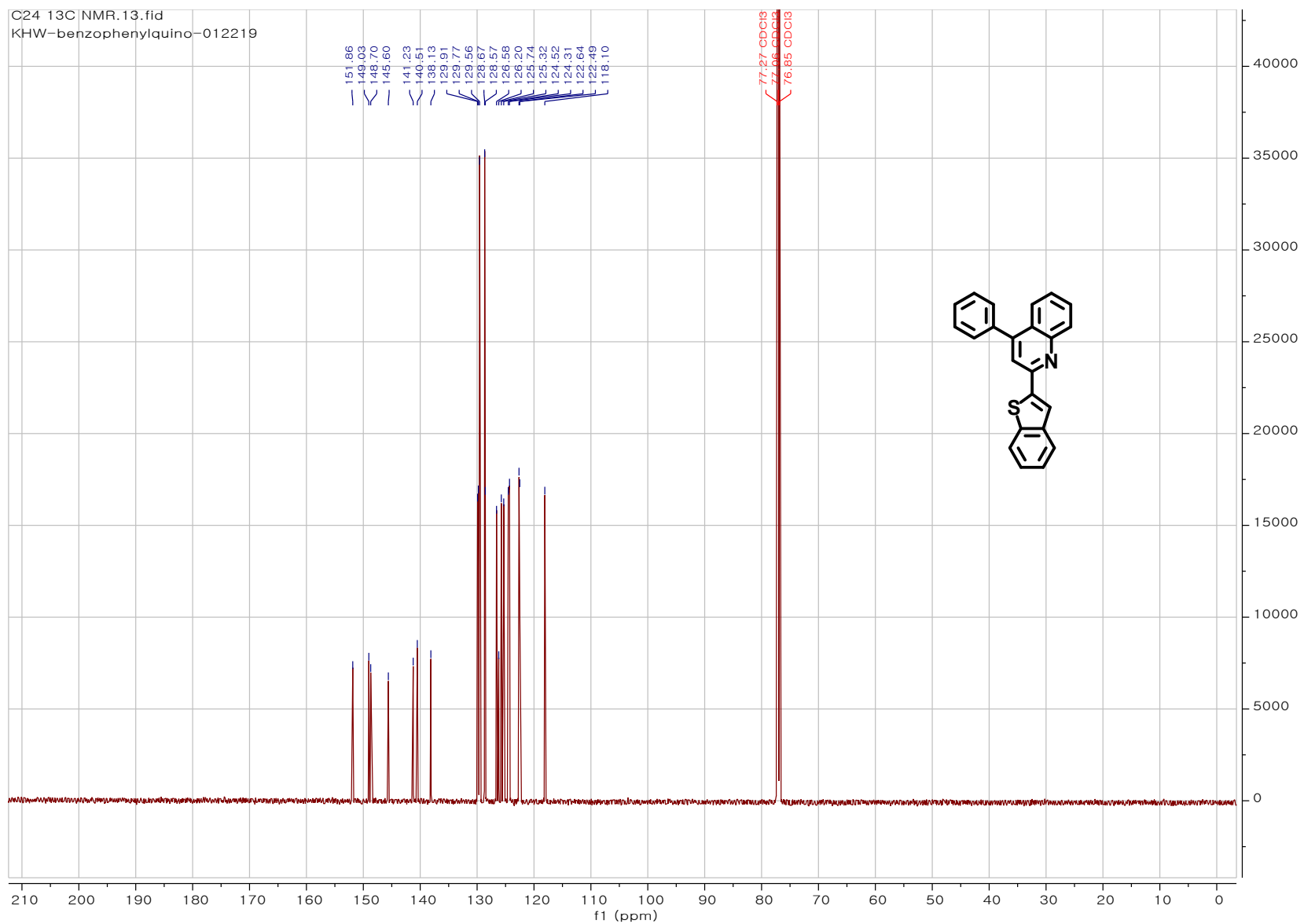


Figure S2 ¹³C-NMR spectrum of 2-(benzo[b]thiophen-2-yl)-4-phenylquinoline (L2).

C24#1-81 RT: 0.00-0.30 AV: 81 NL: 2.19E4
T: ITMS+p ESIsid=35.00 Fullms[150.00-2000.00]

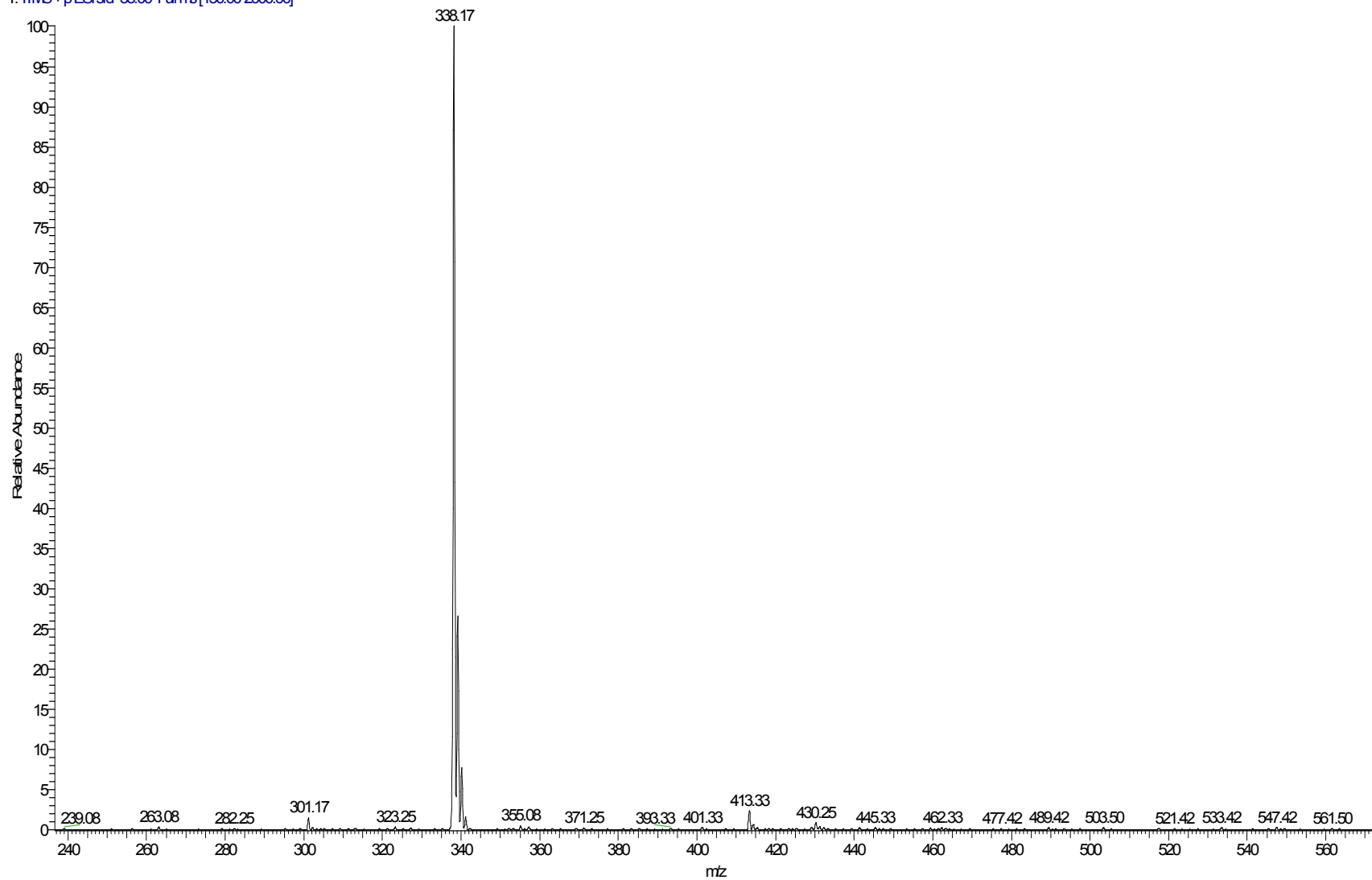


Figure S3 ESI-Mass spectrum of 2-(benzo[b]thiophen-2-yl)-4-phenylquinoline (**L2**).

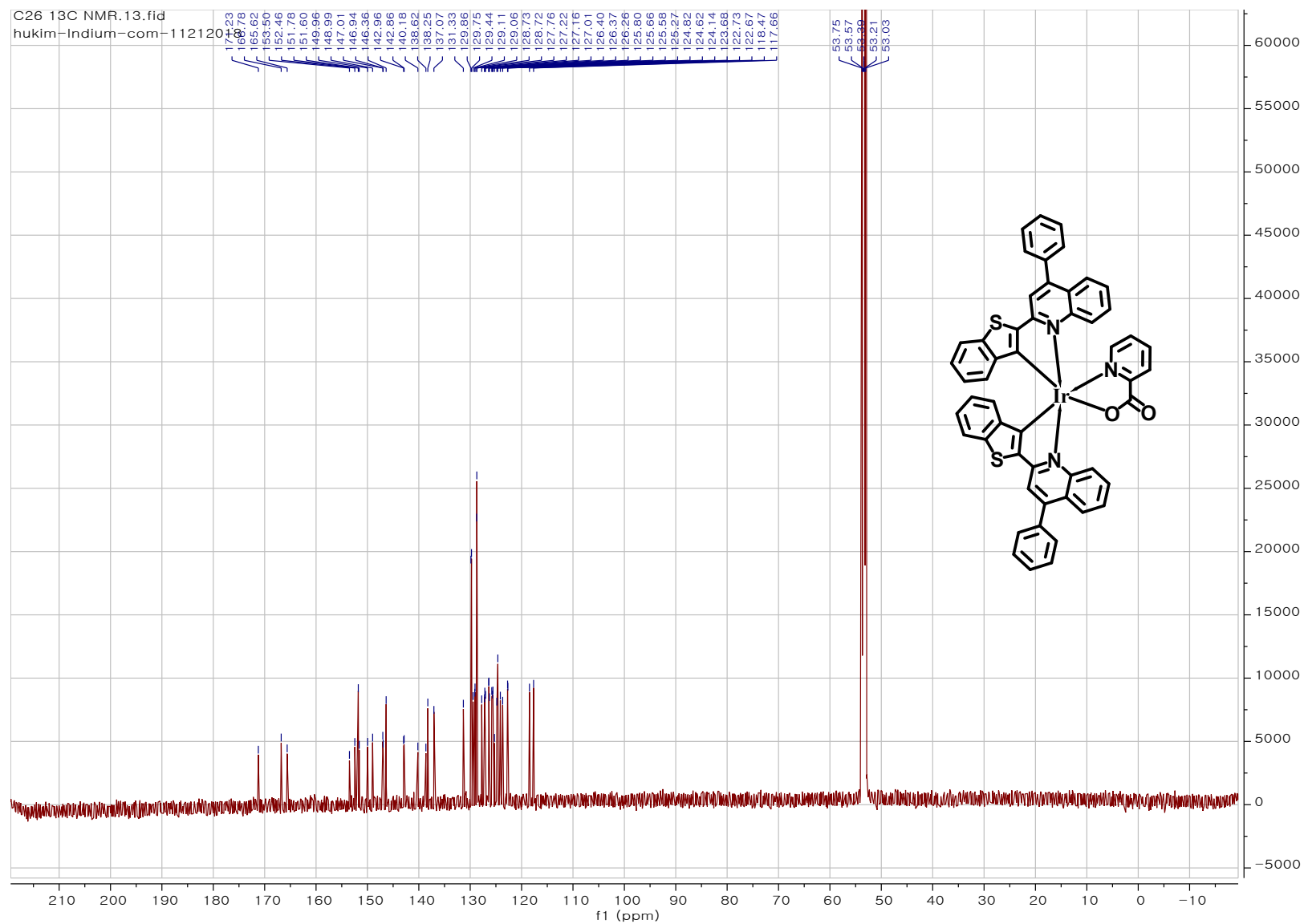


Figure S5 ^{13}C -NMR spectrum of bis[2-(benzo[b]thiophen-2-yl))-4-phenylquinolate]iridium(III) (picolate): $(\text{btpq})_2\text{Ir}(\text{pic})$ (**Ir2**).

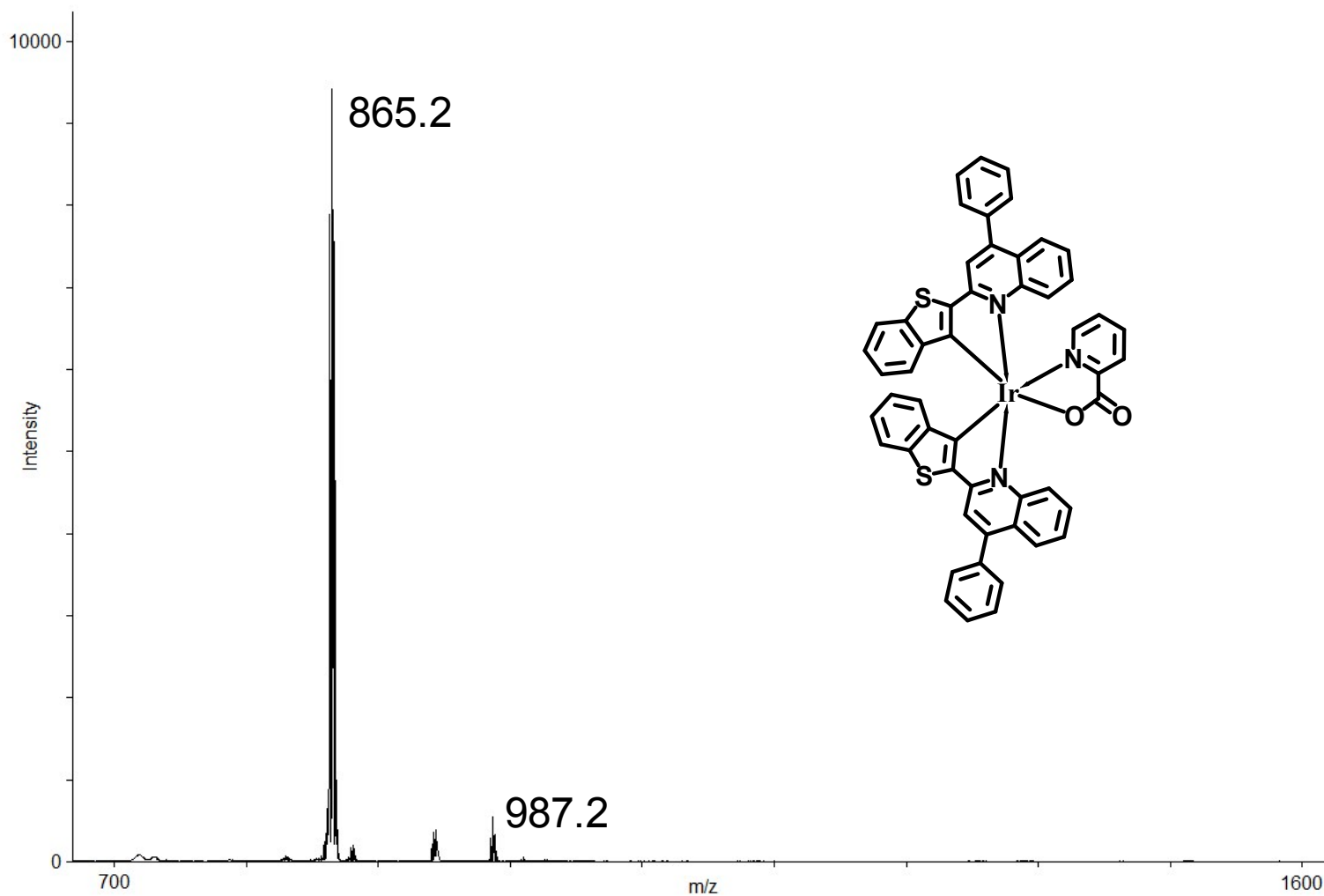


Figure S6 MALDI TOF MASS spectrum of bis[2-(benzo[b]thiophen-2-yl)-4-phenylquinolinate]iridium(III) (picolinate): (btpq)₂Ir(pic) (**Ir2**).

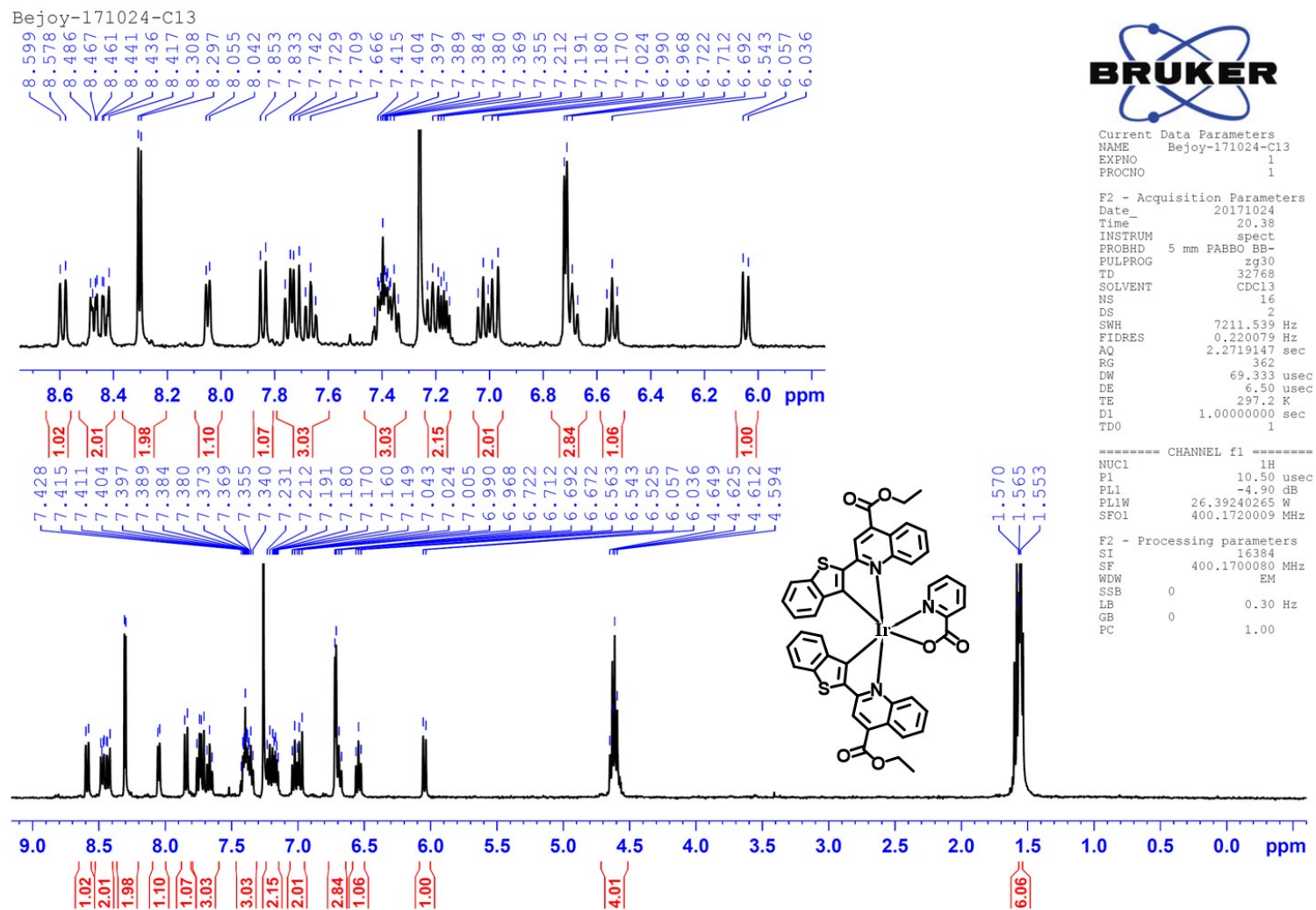


Figure S7 $^1\text{H-NMR}$ spectrum of bis[ethyl 2-(benzo[b]thiophen-2-yl)quinoline-4-carboxylate] iridium(III) (picolate): (btccq) $_2\text{Ir(pic)}$ (**Ir3**).

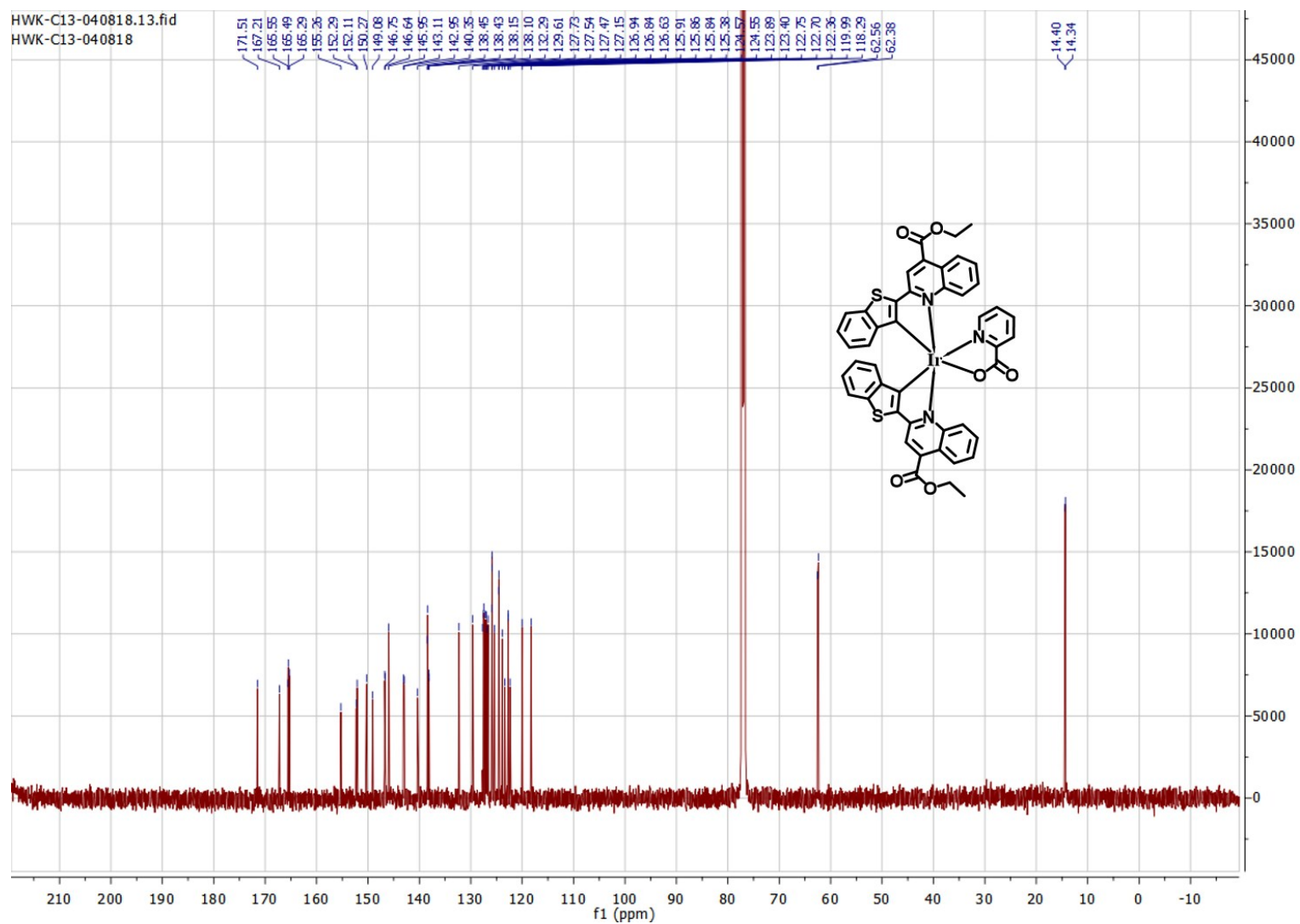


Figure S8 ^{13}C NMR spectrum of bis[ethyl 2-(benzo[b]thiophen-2-yl)quinoline-4-carboxylate] iridium(III) (picolate): $(\text{btecq})_2\text{Ir}(\text{pic})$ (**Ir3**).

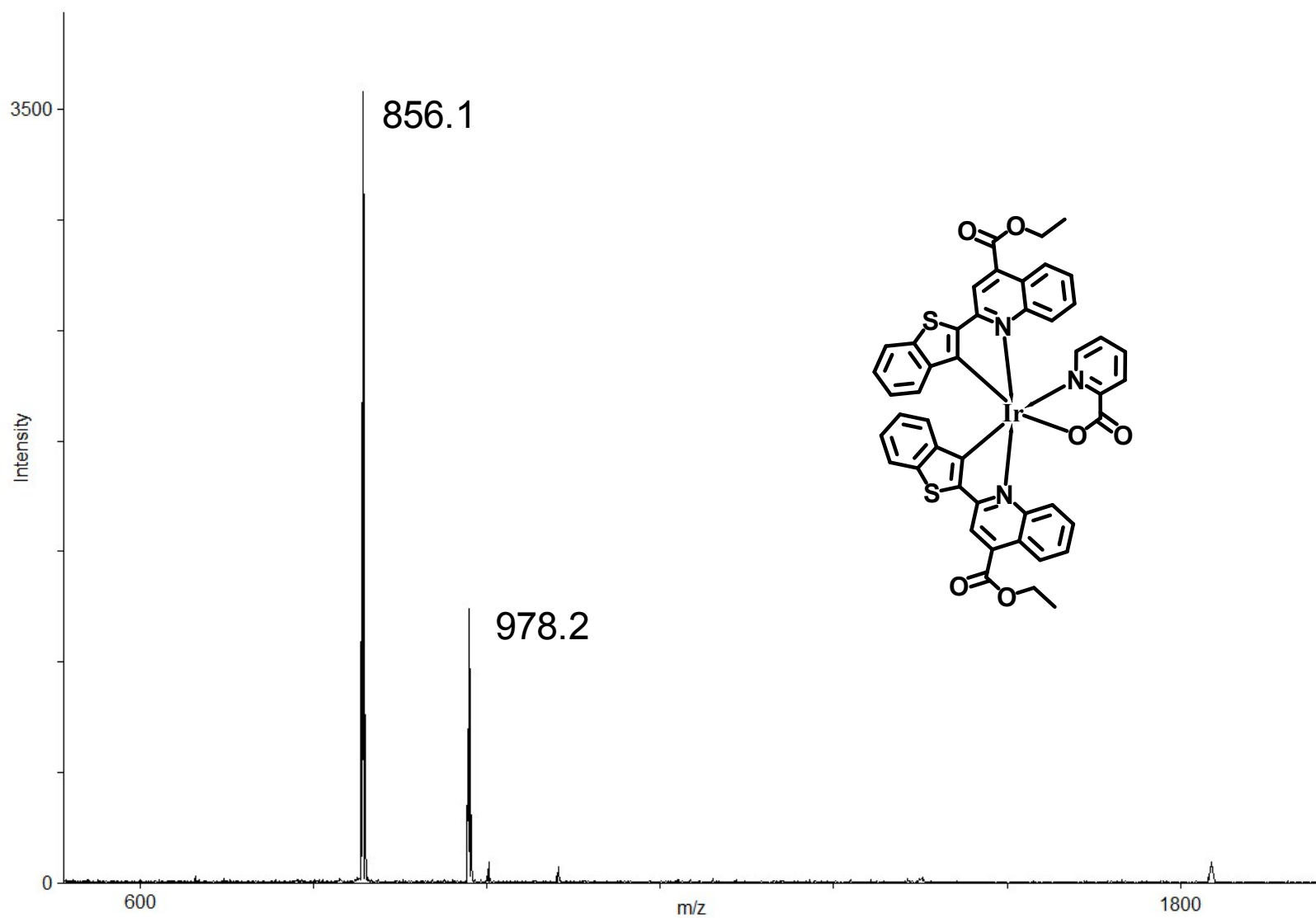


Figure S9 MALDI TOF MASS spectrum of bis[ethyl 2-(benzo[b]thiophen-2-yl)quinoline-4-carboxylate] iridium(III) (picolinate): (btecq)₂Ir(pic) (**Ir3**).

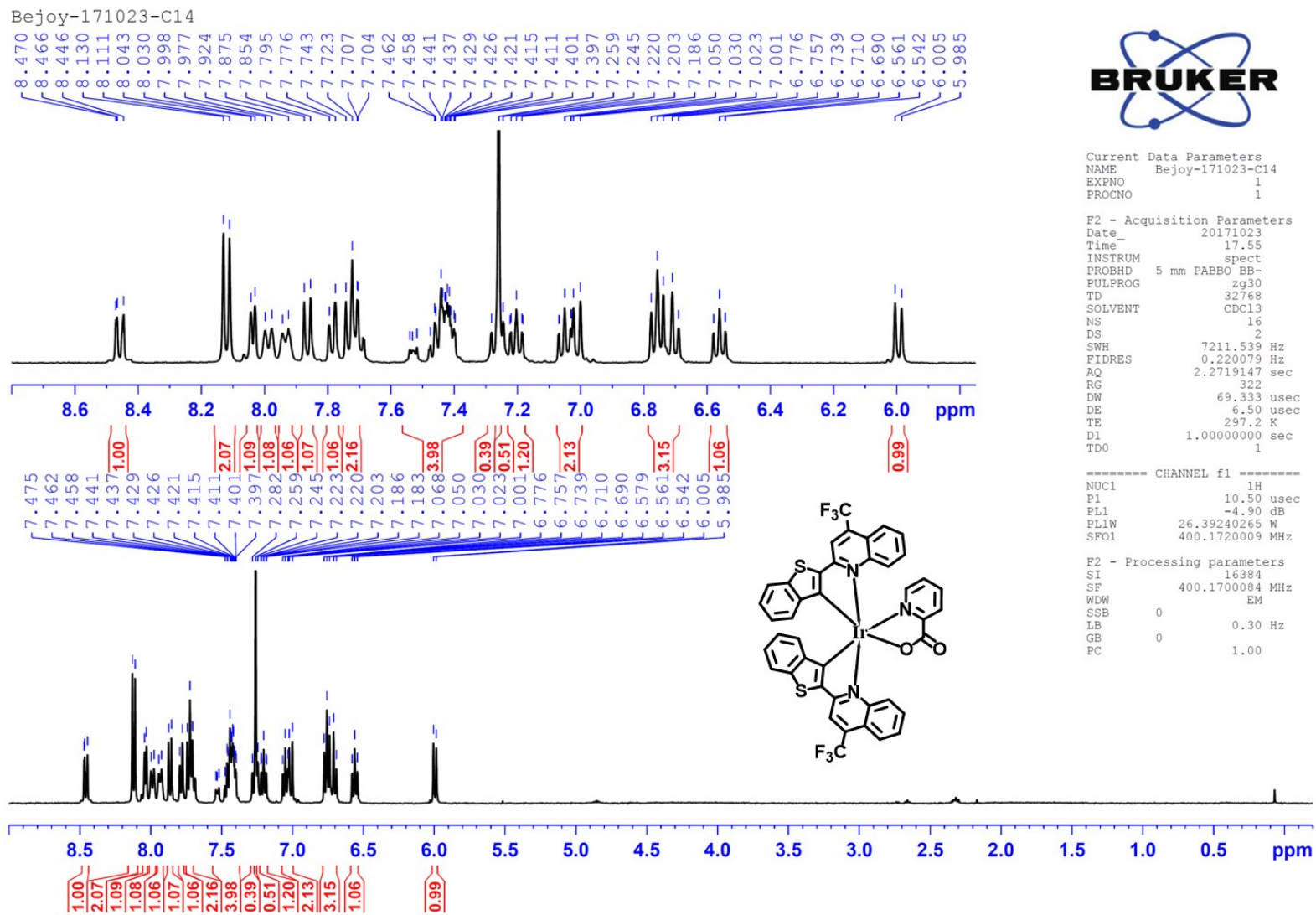


Figure S10 $^1\text{H-NMR}$ spectrum of bis[2-(benzo[b]thiophen-2-yl)-4-(trifluoromethyl)quinoline] iridium(III) (picolinate): (bttmq) $_2$ Ir(pic) (**Ir4**).

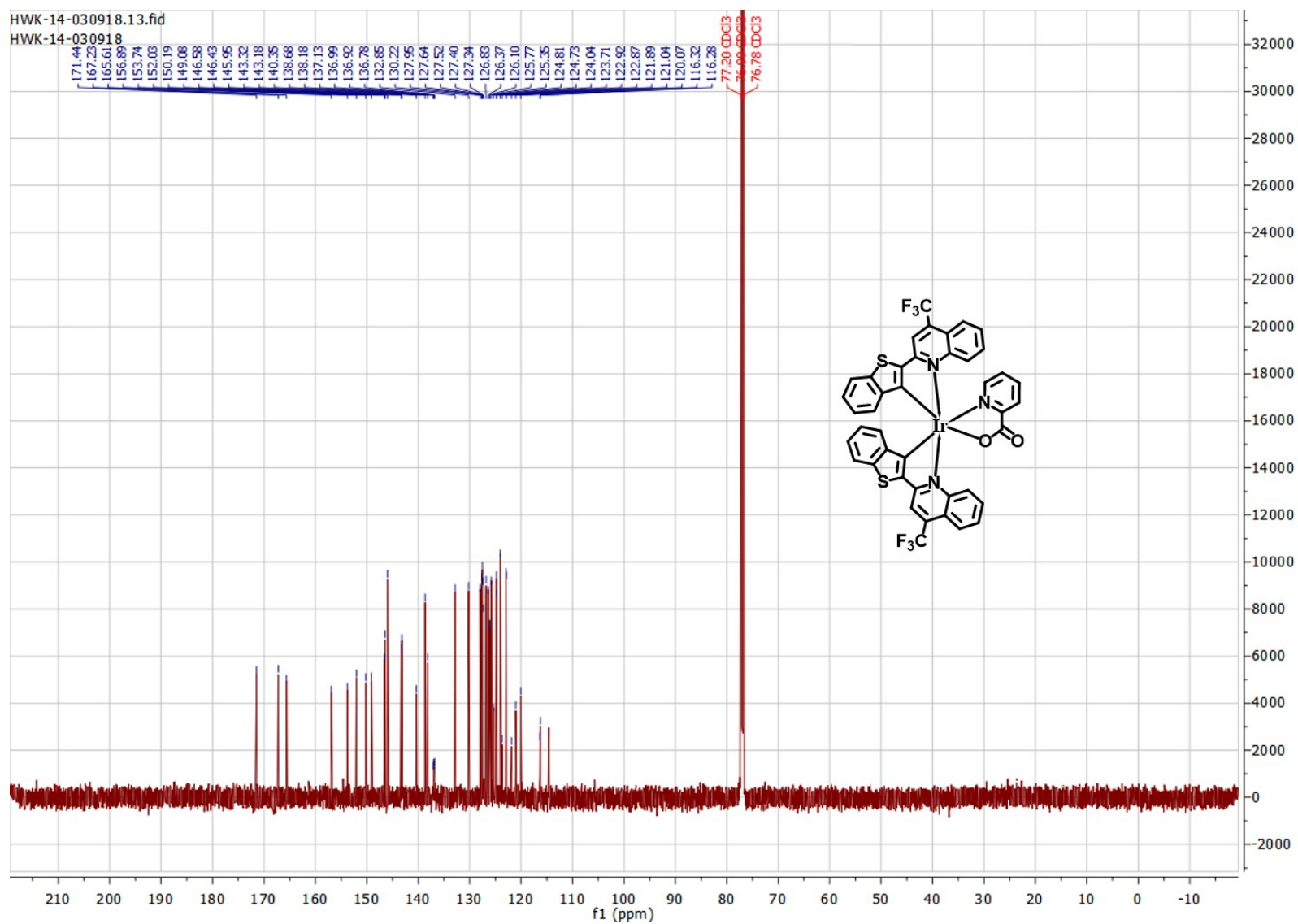


Figure S11 ^{13}C -NMR spectrum of bis[2-(benzo[b]thiophen-2-yl)-4-(trifluoromethyl)quinoline] iridium(III) (picolinate): (bttmq) $_2$ Ir(pic) (**Ir4**).

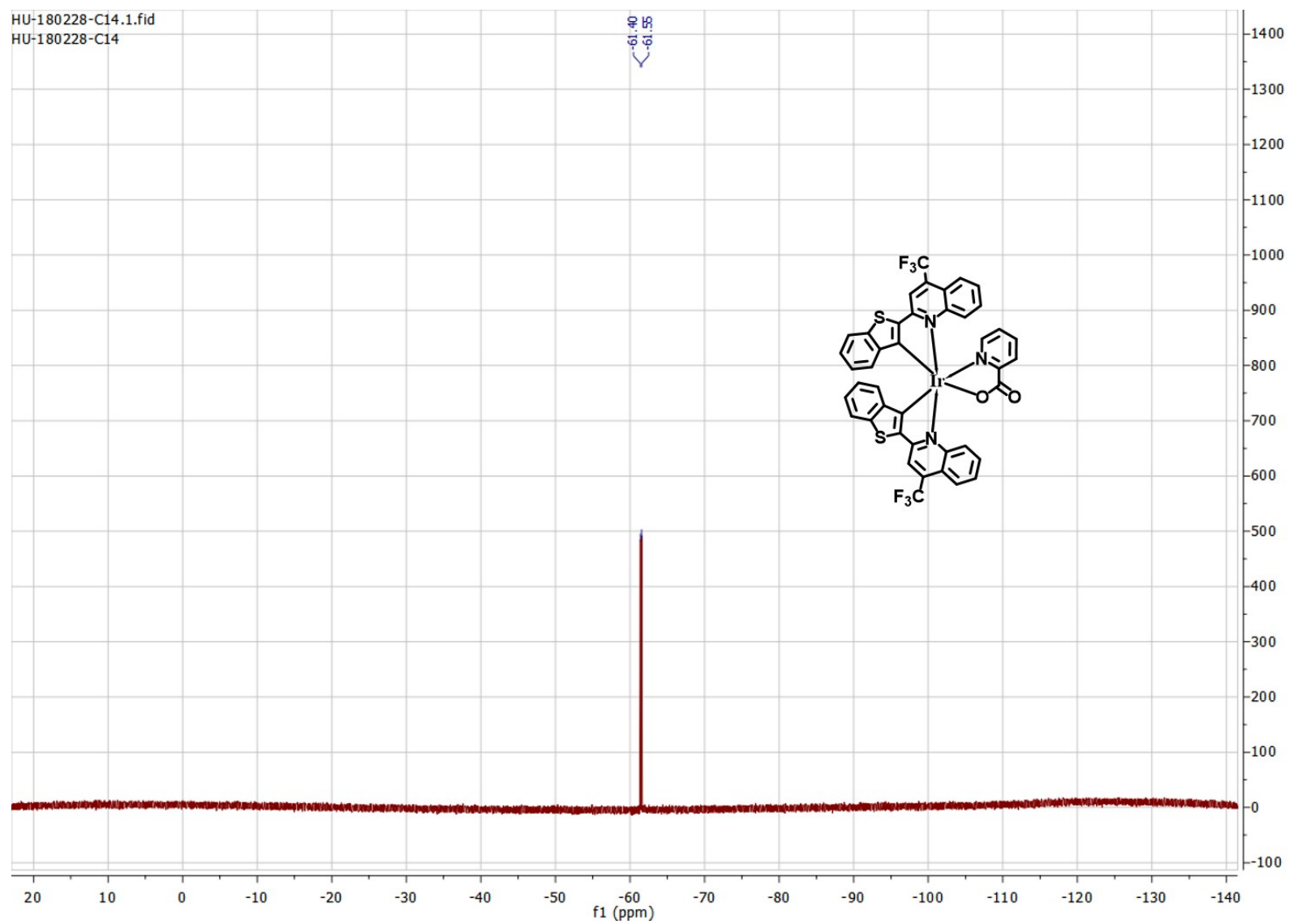


Figure S12 ^{19}F -NMR spectrum of bis[2-(benzo[b]thiophen-2-yl)-4-(trifluoromethyl)quinoline] iridium(III) (picolinate): (bttmq) $_2$ Ir(pic) (**Ir4**).

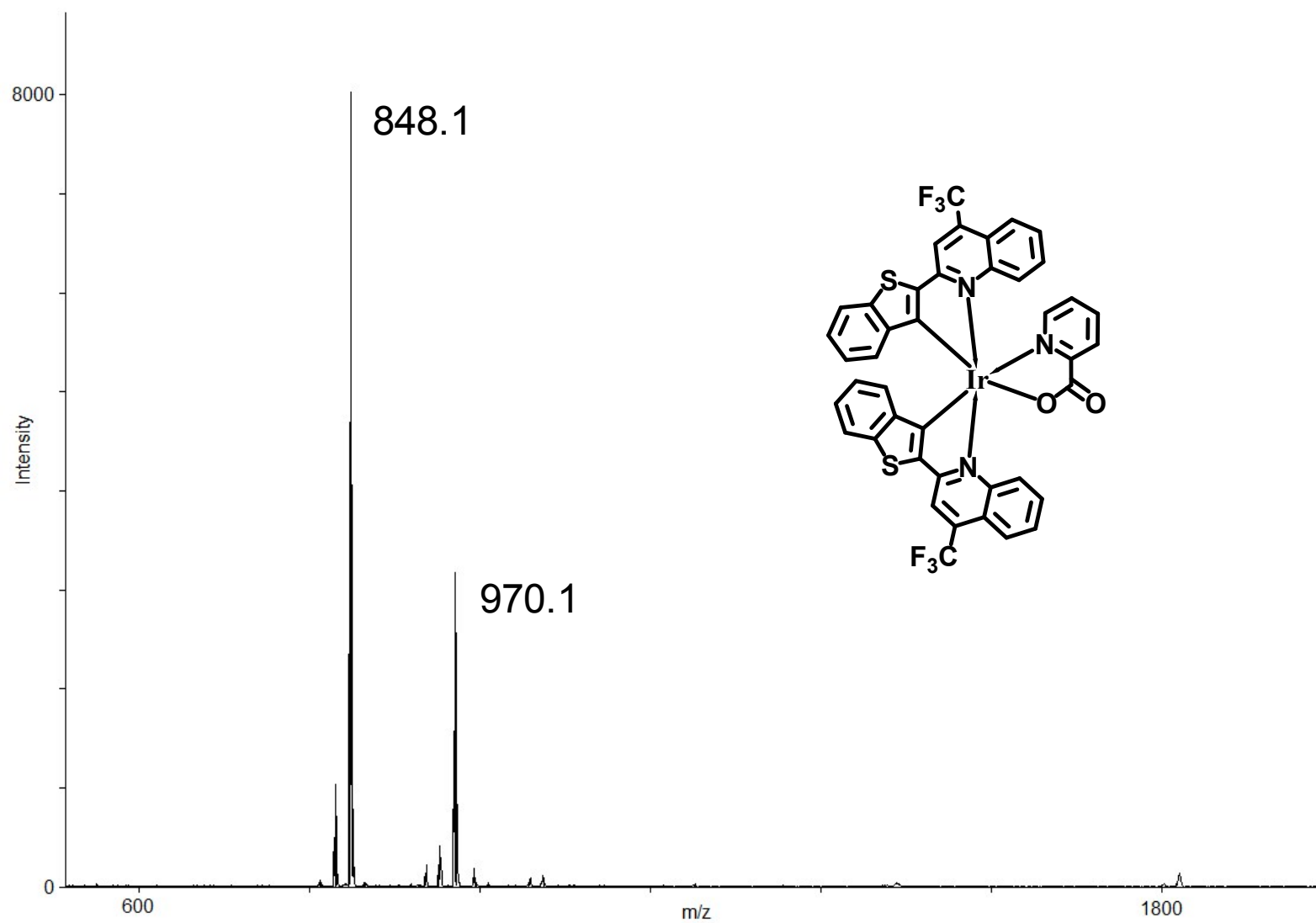


Figure S13 MALDI TOF MASS spectrum of bis[2-(benzo[b]thiophen-2-yl)-4-(trifluoromethyl)quinoline] iridium(III) (picolinate): (bttmq)₂Ir(pic) (**Ir4**).

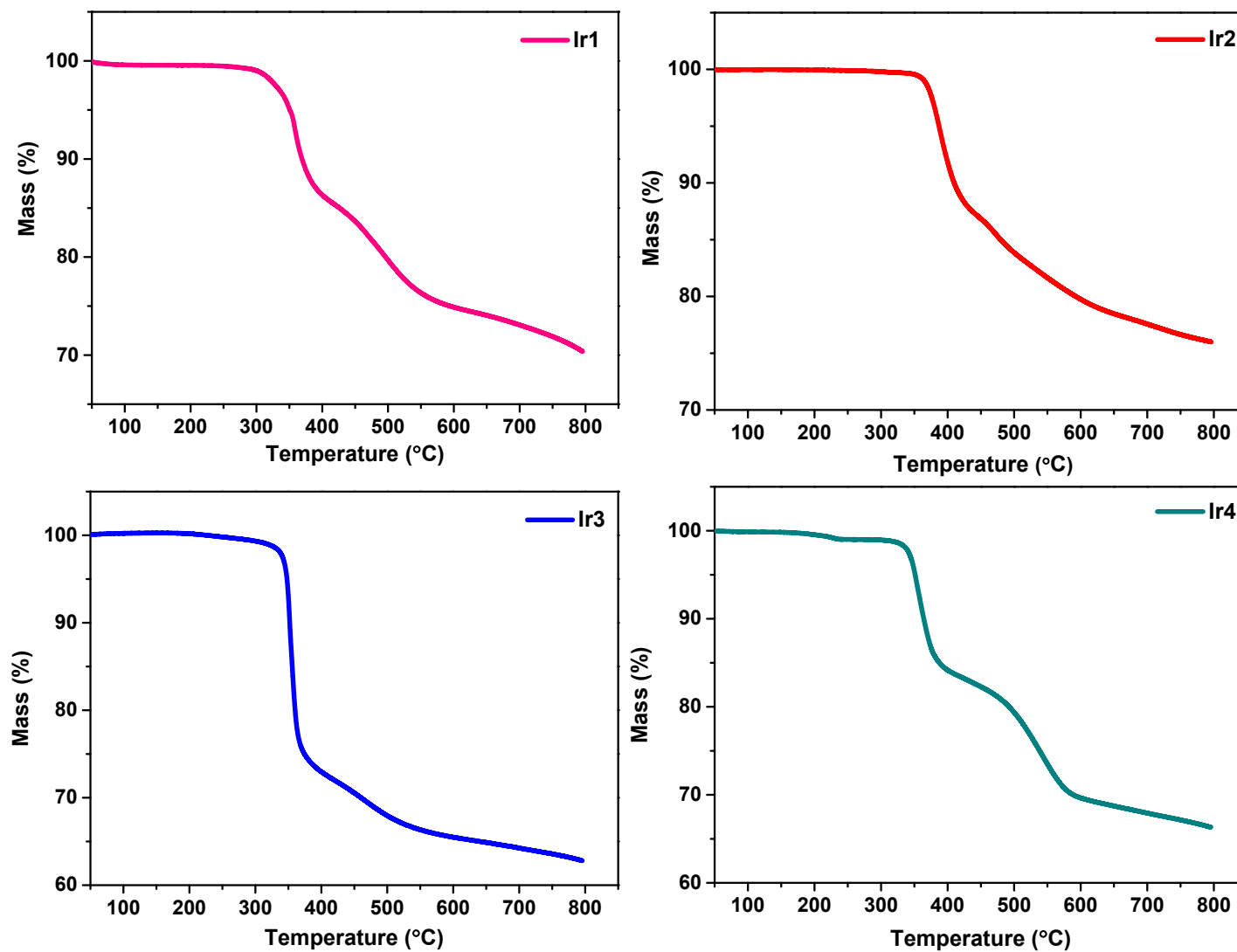


Figure S14 Thermogravimetric curves for complex **Ir1** **Ir4** under nitrogen atmosphere.

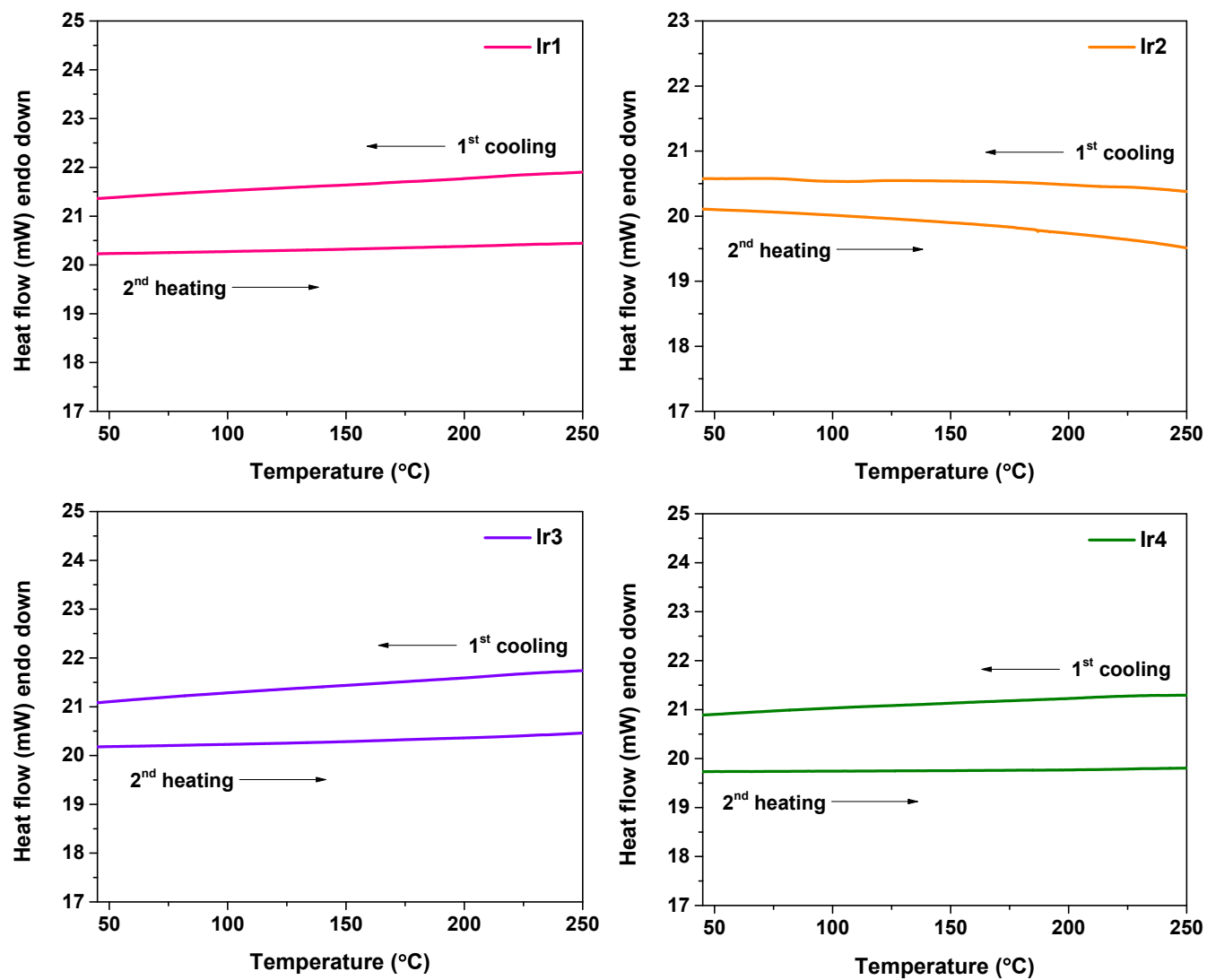
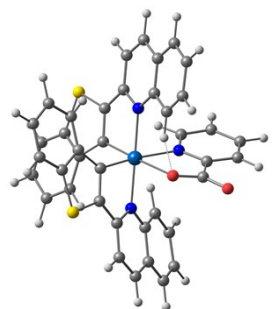
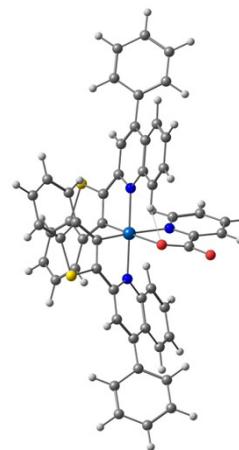


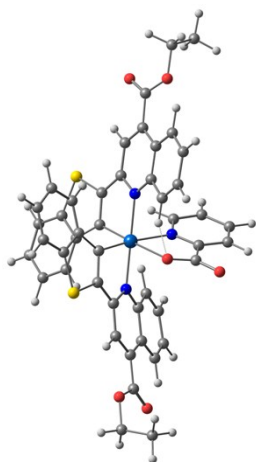
Figure S15 Differential scanning calorimetric curves for complex Ir1 Ir4 under nitrogen atmosphere.



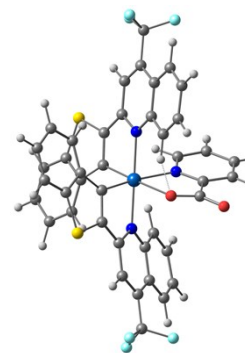
Ir1



Ir2



Ir3



Ir4

Figure S16 Optimized geometries of **Ir1-Ir4** at the PBE1PBE/6-31G* level.

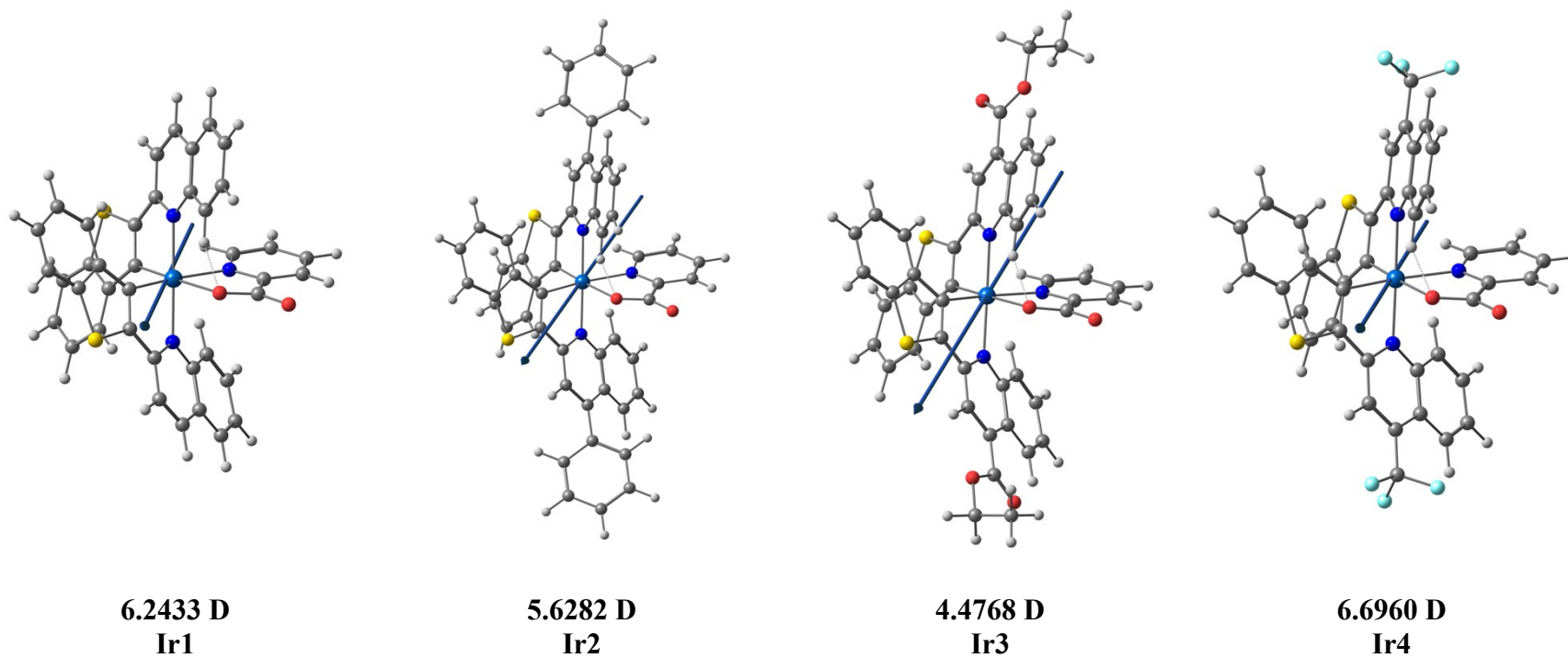


Figure S17 Optimized geometries of Ir1-Ir4 exhibits dipole moment at the PBE1PBE/6-31G* level.

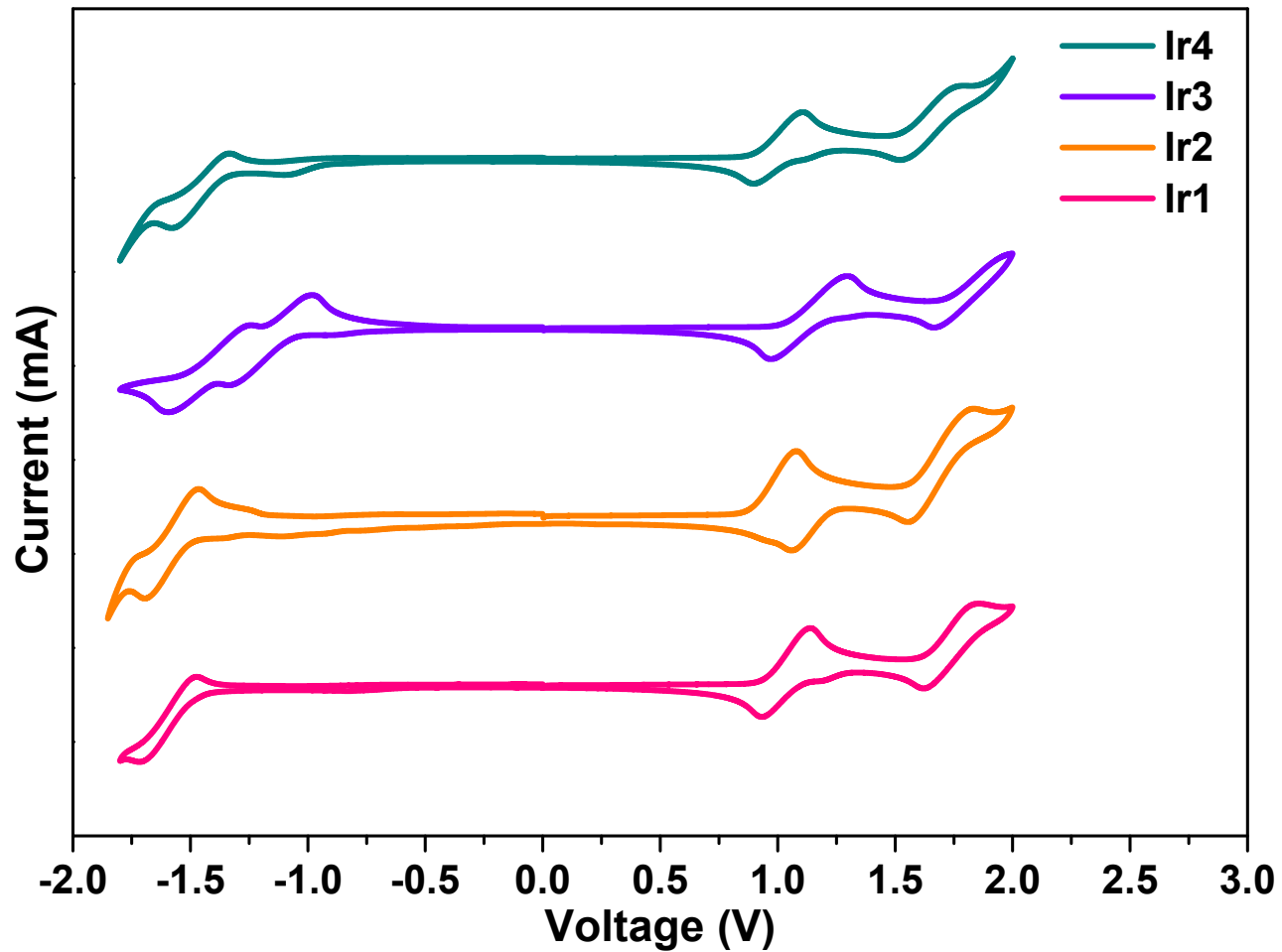


Figure S18 Cyclic voltammograms of redox processes of complexes **Ir1–Ir4** (conditions: GC as working electrode, sweep rate $\nu = 100$ mV/s, 0.2 M Bu_4NPF_6 in CH_2Cl_2 vs Ag/AgCl).

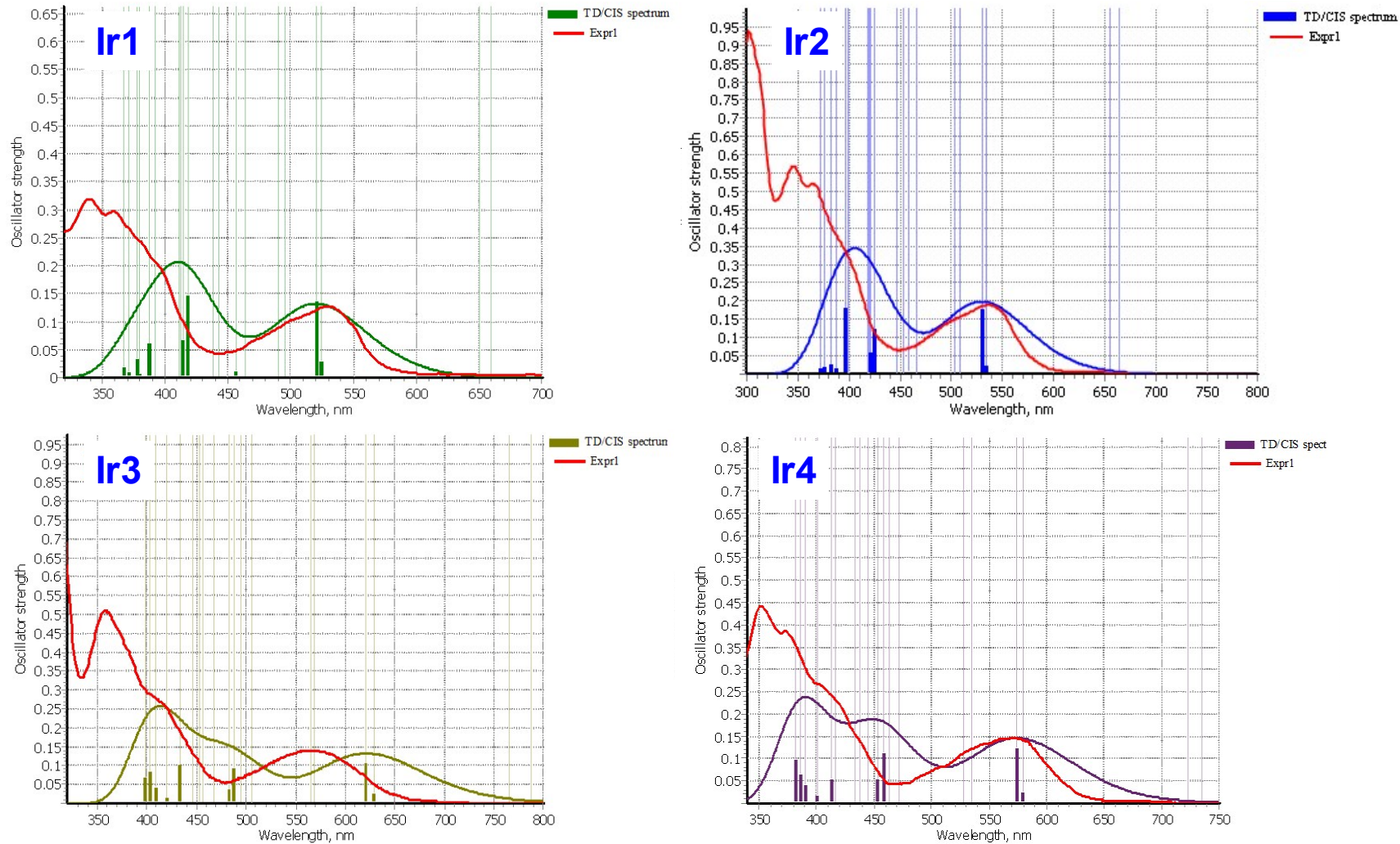


Figure S19 Comparison of experimental (red line) and Calculated absorption spectra (TD-DFT) for **Ir1-Ir4**. The vertical segments are the calculated absorption wavelengths and their size is proportional to the oscillator strength. The calculated spectral lines are the convolution of the transitions with a gaussian smearing of 0.15eV.

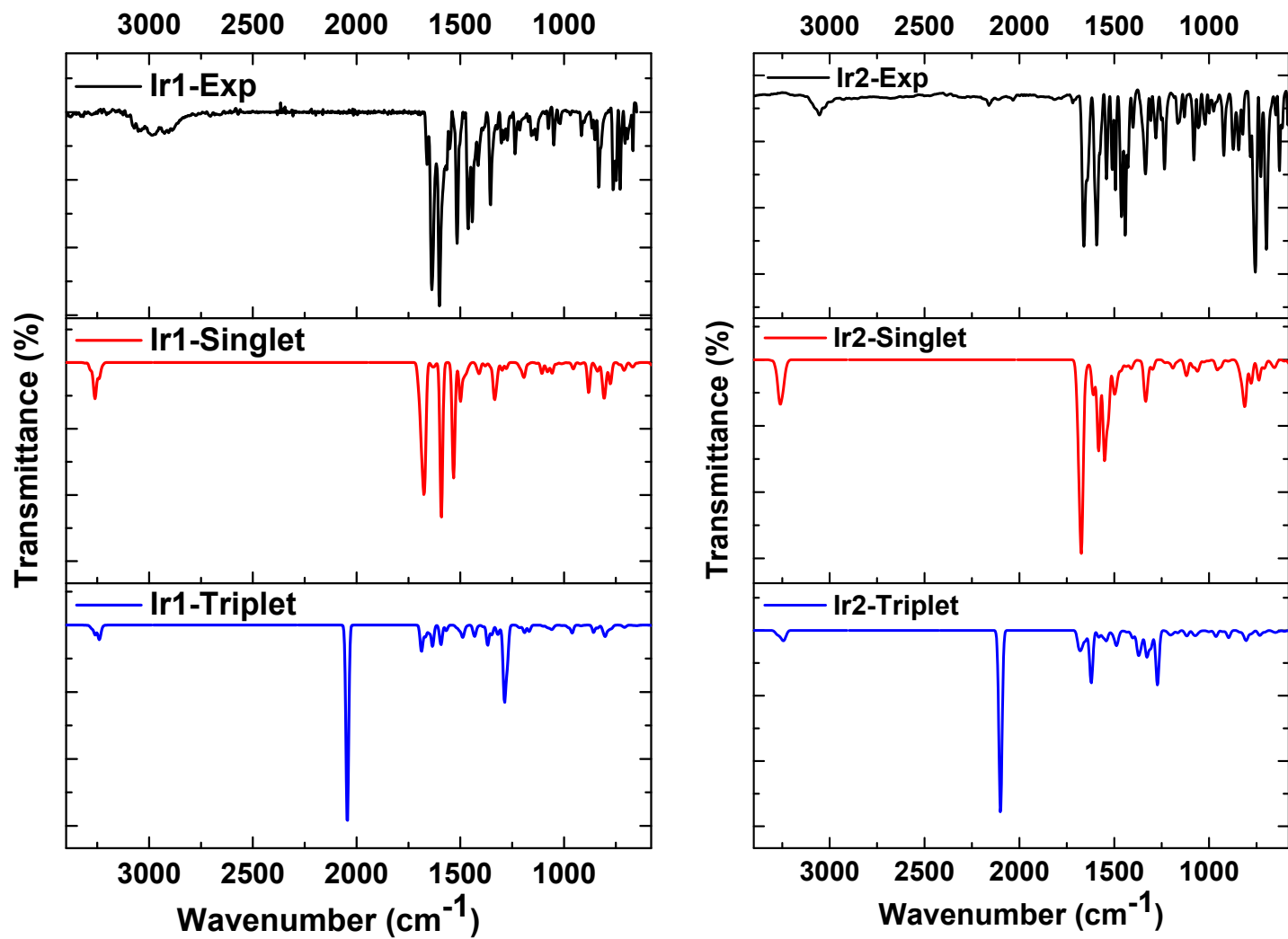


Figure S20 Comparison of experimental FT-IR Spectrum with the IR intensity obtained from the optimized triplet and singlet geometries of **Ir1** and **Ir2**.

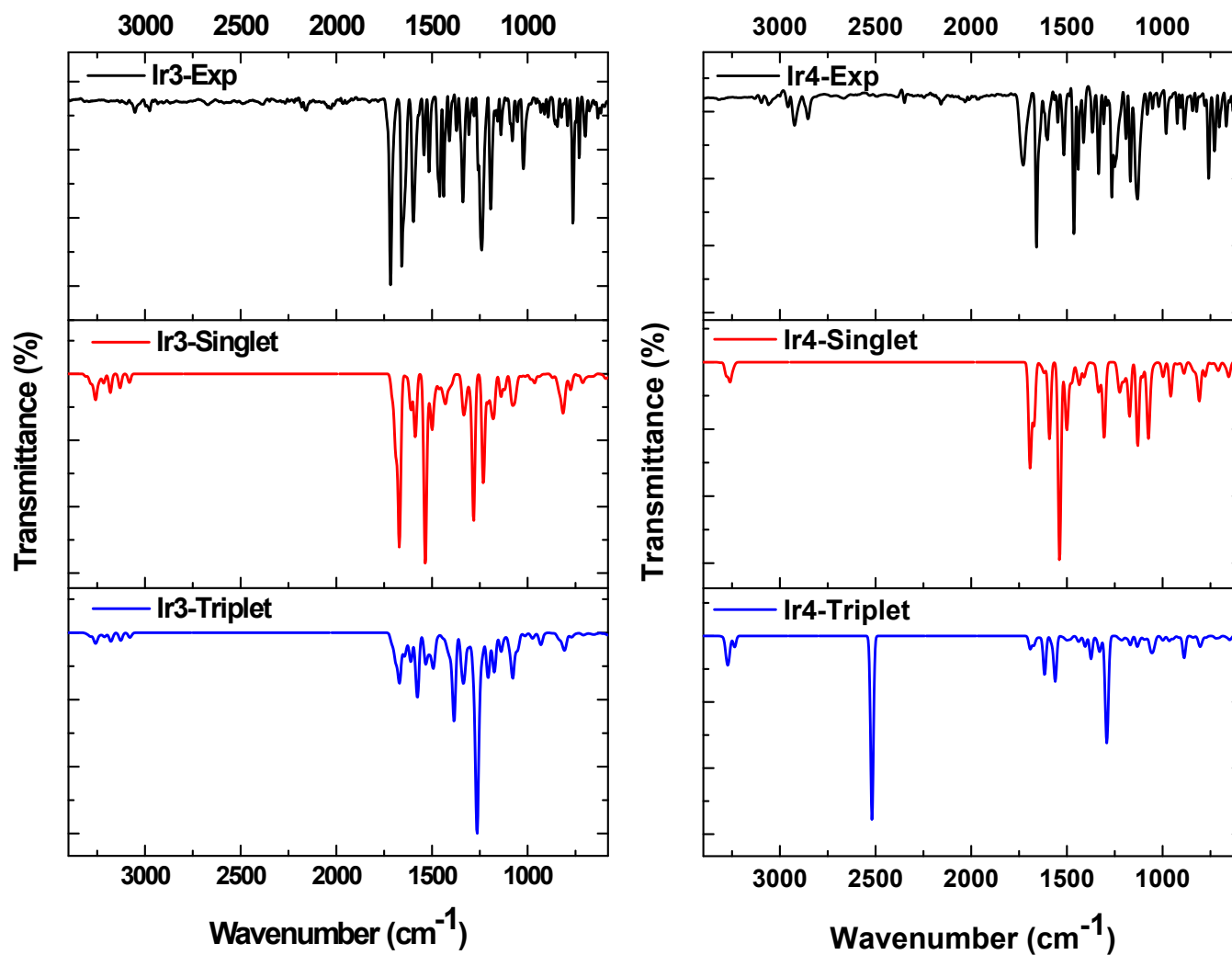


Figure S21 Comparison of experimental FT-IR Spectrum with the IR intensity obtained from the optimized triplet and singlet geometries of **Ir3** and **Ir4**.

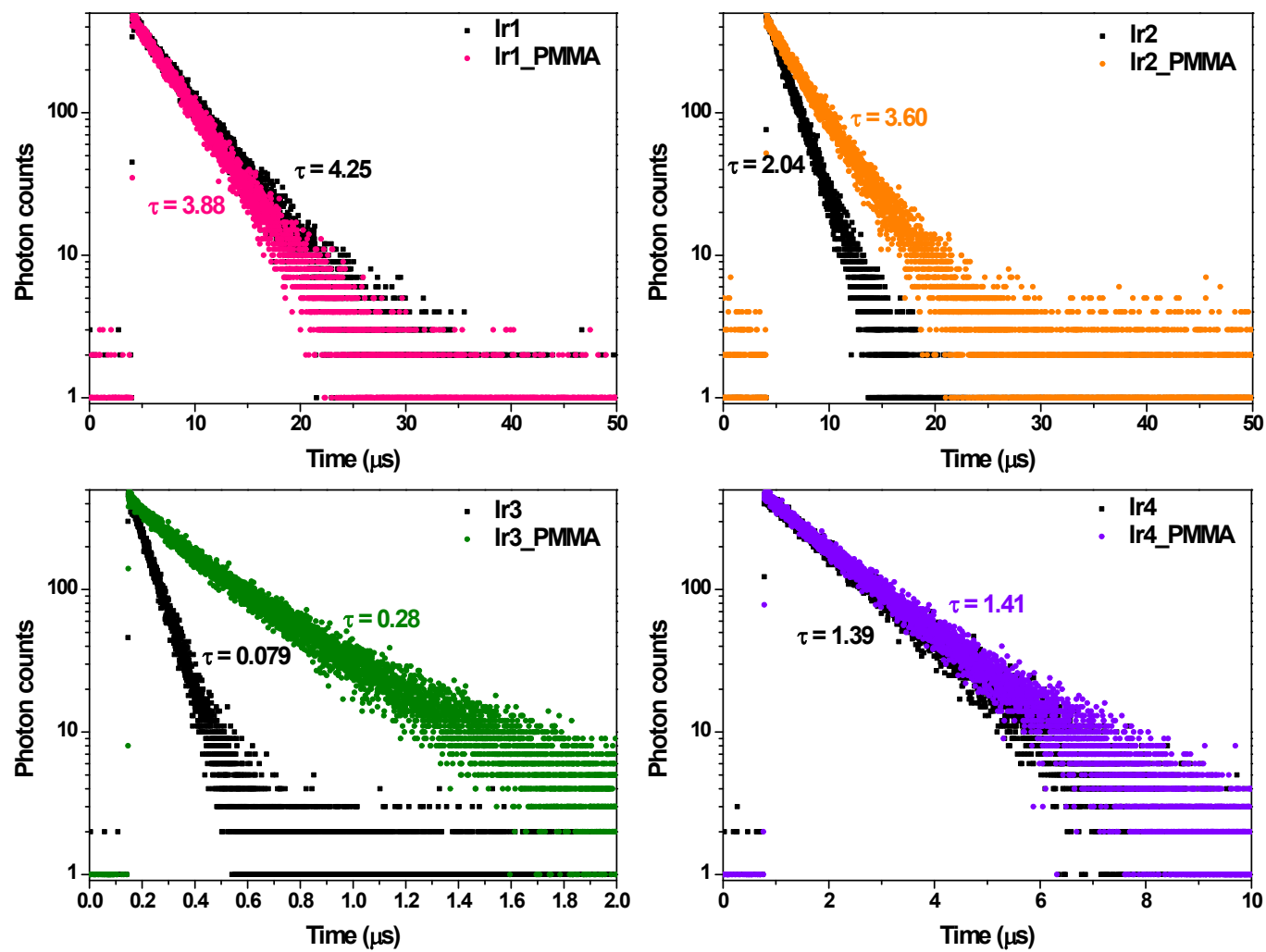


Figure S22 Comparison of lifetime decay profiles of complex **Ir1**–**Ir4** in degassed dichloromethane solution ($c = 2 \times 10^{-5}$ M) and 5 wt% doped PMMA films at 298 K ($\lambda_{\text{exc}} = 464$ nm).

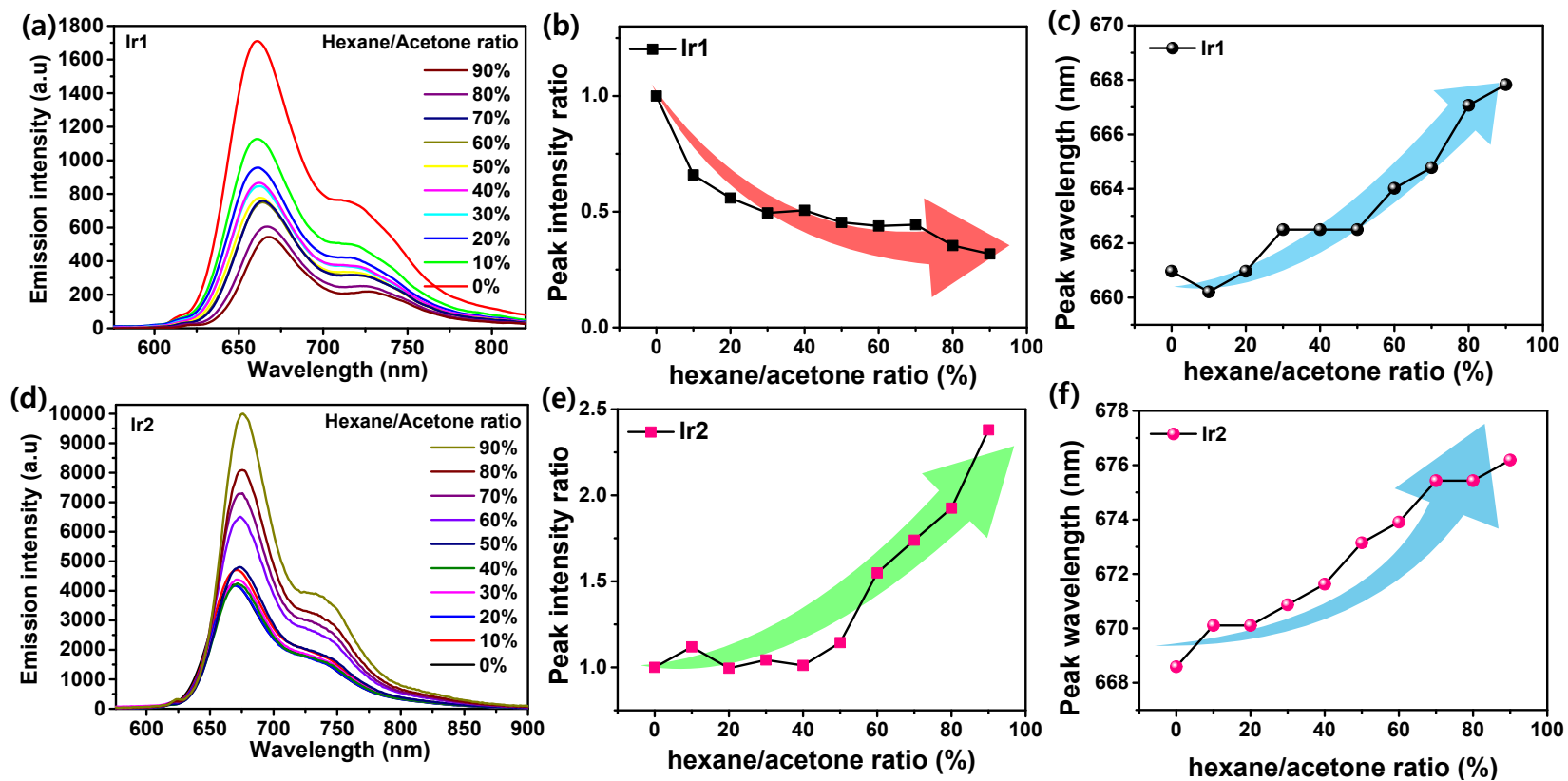


Figure S23 Emission spectrum of (a) **Ir1** and (d) **Ir2** ($c = 5 \mu\text{M}$) in acetone–hexane mixtures with increasing hexane fractions (0–90%) at room temperature. Variation of Peak intensity ratio of (b) **Ir1** and (e) **Ir2** with respect to hexane fractions. Peak wavelength change in (c) **Ir1** and (f) **Ir2** corresponding to the increasing hexane fractions.

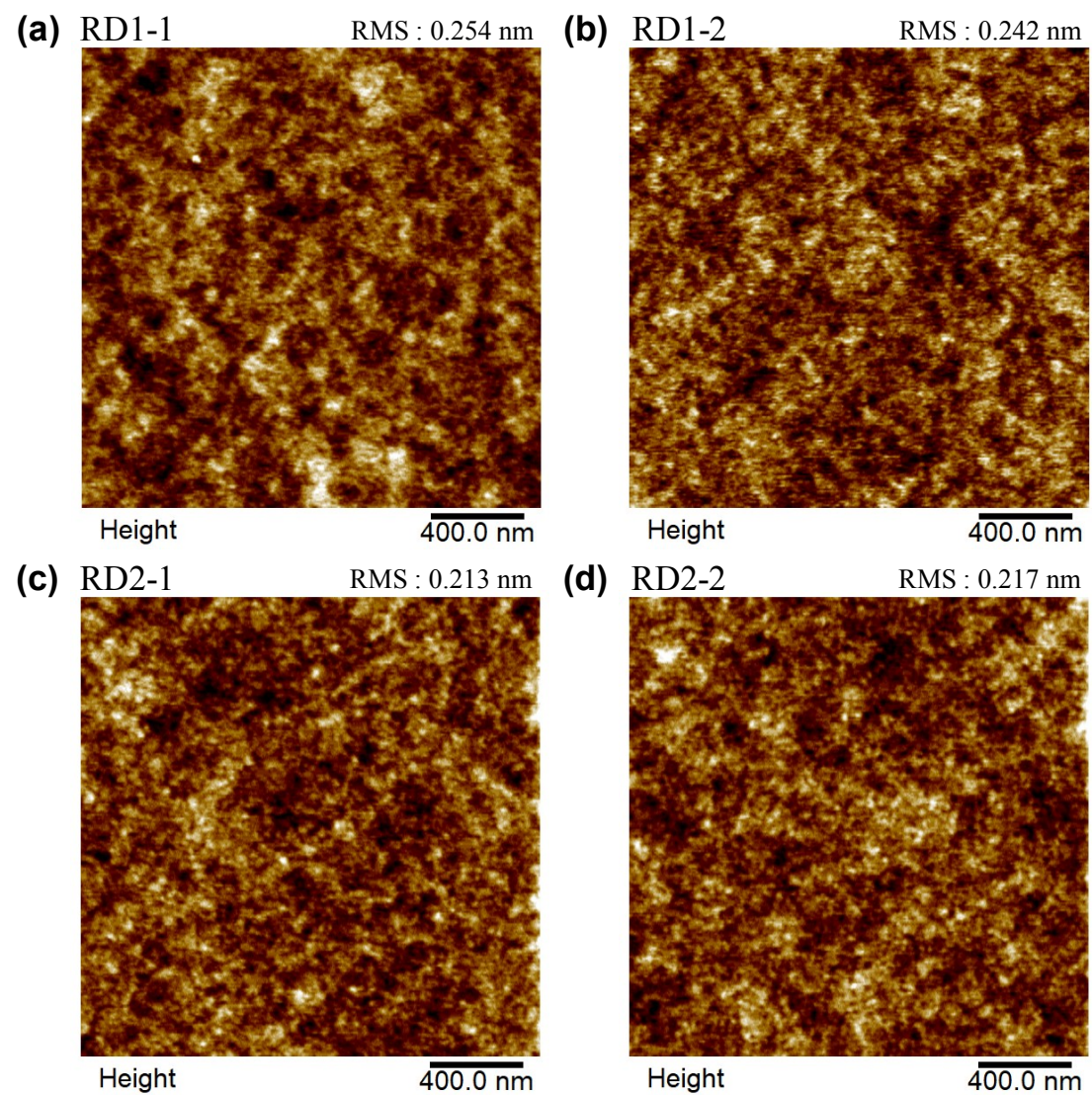


Figure S24 Two-dimensional (top) and three-dimensional (bottom) AFM images of emissive layers of RD1-1, RD1-2, RD2-1 and RD2-2. (Scan sizes are $3 \times 3 \mu\text{m}$ for all films).

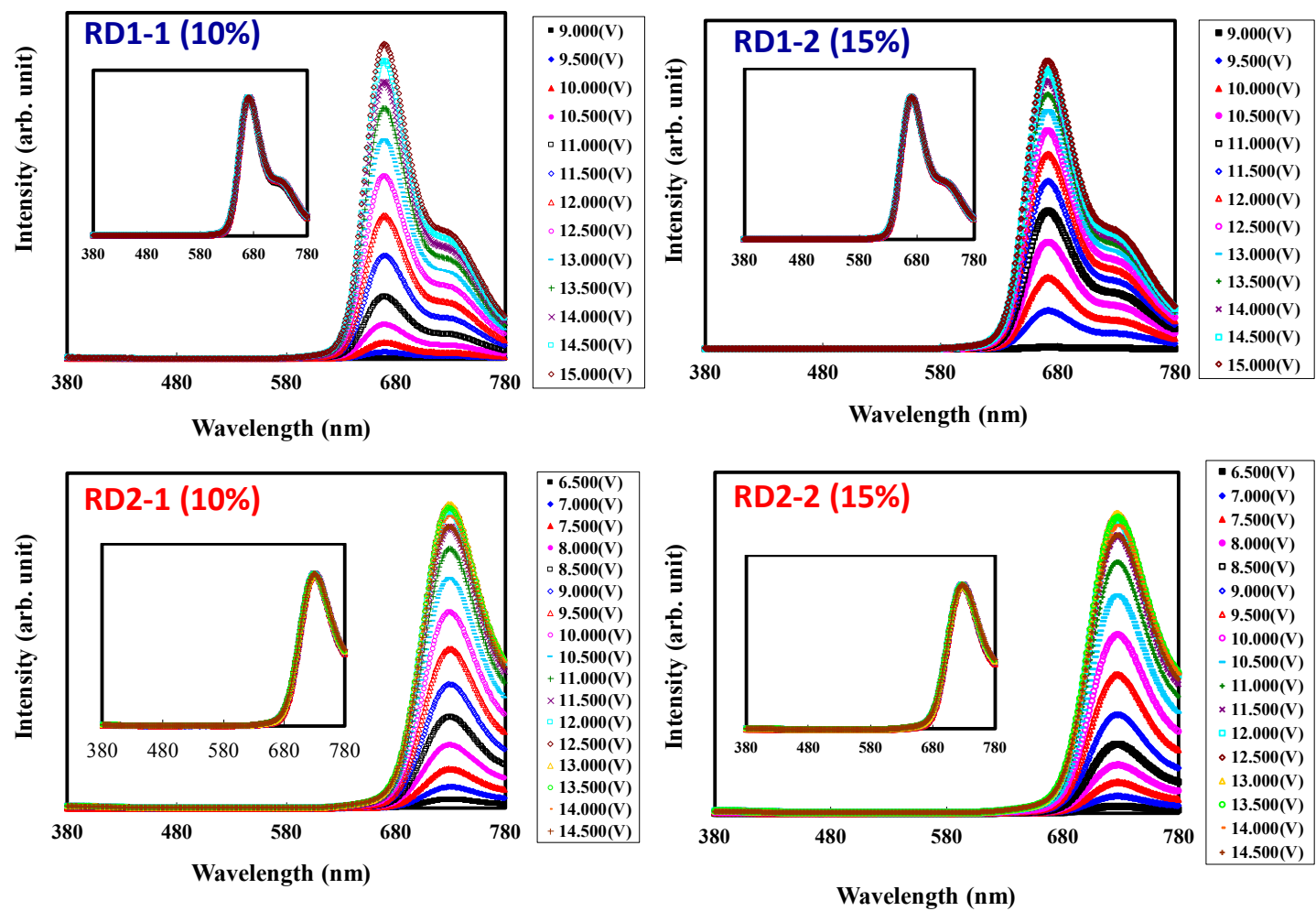


Figure S25 Electroluminescence spectra (inset: normalized spectra) from (a) RD1-1, (b) RD1-2, (c) RD2-1 and (d) RD2-2 PhOLEDs as a function of applied voltages during operation.

Table S1 Selected Bond Lengths for Complexes **Ir1-Ir4**.

Selected bond lengths for Ir1 (Å)			
Number	Atom1	Atom2	Length
1	C16	Ir1	1.979(4)
2	C33	Ir1	1.996(3)
3	N1	Ir1	2.086 (8)
4	N2	Ir1	2.101 (8)
5	N3	Ir1	2.136 (6)
6	O1	Ir1	2.145 (7)
Selected bond lengths for Ir2 (Å)			
1	C22	Ir1	1.993(2)
2	C45	Ir1	2.006(2)
3	N1	Ir1	2.147(2)
4	N2	Ir1	2.091(2)
5	N3	Ir1	2.102(2)
6	O1	Ir1	2.156(2)
Selected bond lengths for Ir3 (Å)			
1	C19	Ir1	2.009(2)
2	C39	Ir1	1.983(2)
3	N1	Ir1	2.146(2)
4	N2	Ir1	2.099(2)
5	N3	Ir1	2.064(2)
6	O1	Ir1	2.154(1)
Selected bond lengths for Ir4 (Å)			
1	C17	Ir1	1.995(4)
2	C35	Ir1	1.962(4)
3	N1	Ir1	2.153(3)
4	N2	Ir1	2.097(4)
5	N3	Ir1	2.075(4)
6	O1	Ir1	2.131(3)

Table S2 Selected Bond Angles for **Ir1** and **Ir2**.

Selected bond angles for Ir1 (°)					Selected bond angles for Ir2 (°)				
Number	Atom1	Atom2	Atom3	Angle	Number	Atom1	Atom2	Atom3	Angle
1	C16	Ir1	C33	93.8(1)	1	C22	Ir1	C45	95.5(1)
2	C16	Ir1	N1	97.2(1)	2	C22	Ir1	N1	96.25(9)
3	C16	Ir1	N2	79.9(1)	3	C22	Ir1	N2	79.80(9)
4	C16	Ir1	N3	99.9(1)	4	C22	Ir1	N3	99.43(9)
5	C16	Ir1	O1	173.2(1)	5	C22	Ir1	O1	172.13(9)
6	C33	Ir1	N1	168.7(1)	6	C45	Ir1	N1	168.12(9)
7	C33	Ir1	N2	97.7(1)	7	C45	Ir1	N2	96.76(9)
8	C33	Ir1	N3	79.8(1)	8	C45	Ir1	N3	80.06(9)
9	C33	Ir1	O1	93.0(1)	9	C45	Ir1	O1	91.81(9)
10	N1	Ir1	N2	82.2(1)	10	N1	Ir1	N2	83.33(8)
11	N1	Ir1	N3	100.3(1)	11	N1	Ir1	N3	99.99(8)
12	N1	Ir1	O1	76.0(1)	12	N1	Ir1	O1	76.62(8)
13	N2	Ir1	N3	177.5(1)	13	N2	Ir1	N3	176.66(9)
14	N2	Ir1	O1	99.6(1)	14	N2	Ir1	O1	102.38(8)
15	N3	Ir1	O1	81.0(1)	15	N3	Ir1	O1	78.83(8)

Table S3 Selected Bond Angles for **Ir3** and **Ir4**.

Selected bond angles for Ir3 (°)					Selected bond angles for Ir4 (°)				
Number	Atom1	Atom2	Atom3	Angle	Number	Atom1	Atom2	Atom3	Angle
1	C19	Ir1	C39	94.96(7)	1	C17	Ir1	C35	95.3(2)
2	C19	Ir1	N1	169.23(7)	2	C17	Ir1	O1	92.4(1)
3	C19	Ir1	N2	80.30(7)	3	C17	Ir1	N1	168.5(1)
4	C19	Ir1	N3	94.80(7)	4	C17	Ir1	N2	80.1(1)
5	C19	Ir1	O1	92.80(6)	5	C17	Ir1	N3	96.5(1)
6	C39	Ir1	N1	95.75(7)	6	C35	Ir1	O1	172.3(1)
7	C39	Ir1	N2	101.54(7)	7	C35	Ir1	N1	96.0(1)
8	C39	Ir1	N3	79.96(7)	8	C35	Ir1	N2	99.8(1)
9	C39	Ir1	O1	172.20(7)	9	C35	Ir1	N3	80.2(1)
10	N1	Ir1	N2	98.68(6)	10	O1	Ir1	N1	76.2(1)
11	N1	Ir1	N3	85.91(6)	11	O1	Ir1	N2	81.6(1)
12	N1	Ir1	O1	76.51(6)	12	O1	Ir1	N3	98.8(1)
13	N2	Ir1	N3	174.96(6)	13	N1	Ir1	N2	99.7(1)
14	N2	Ir1	O1	78.95(5)	14	N1	Ir1	N3	83.6(1)
15	N3	Ir1	O1	100.23(6)	15	N2	Ir1	N3	176.6(1)

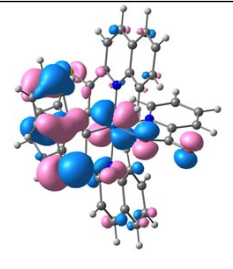
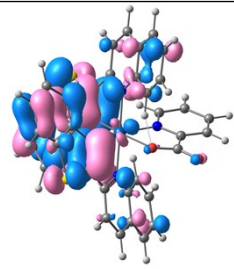
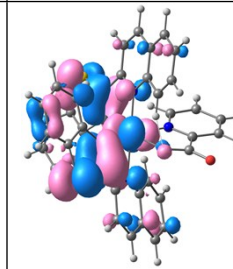
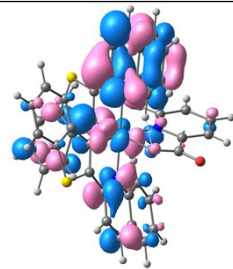
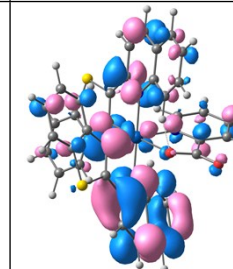
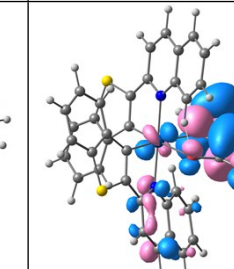
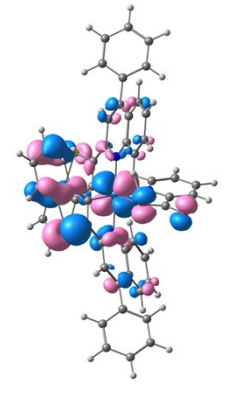
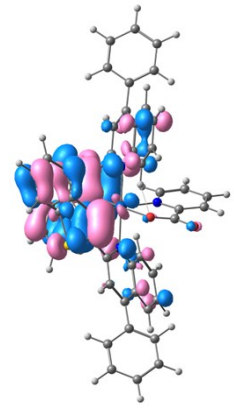
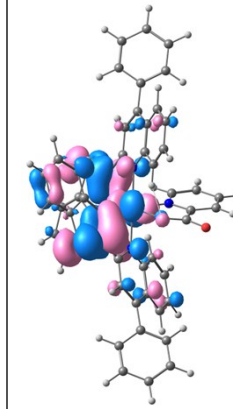
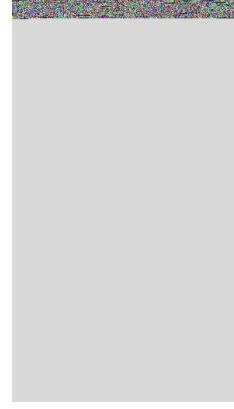
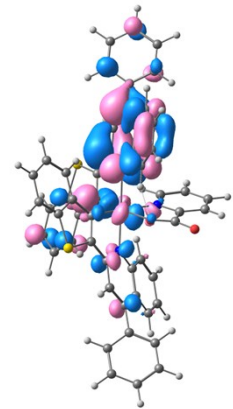
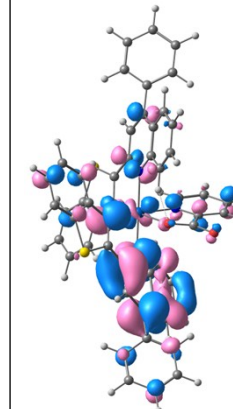
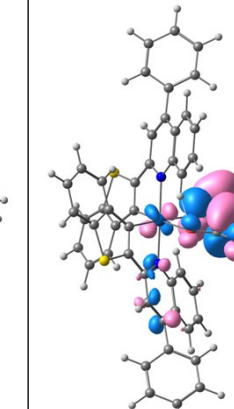
Table S4. Crystallographic and refinement data for complexes **Ir2-Ir4**.

	Ir2	Ir3	Ir4
Formula	(C ₅₂ H ₃₂ Ir N ₃ O ₂ S ₂), (C H Cl ₃) _{1.937}	(C ₄₆ H ₃₂ Ir N ₃ O ₆ S ₂), (C H ₂ Cl ₂) _{0.372}	(C ₄₂ H ₂₂ F ₆ Ir N ₃ O ₂ S ₂) ₂ , (C H ₂ Cl ₂) _{2.674}
Formula weight	1217.00	1010.91	2167.72
Temp (K)	100	100	100
Wavelength (Å)	0.71073	0.620	0.620
Crystal system	monoclinic	monoclinic	triclinic
Space group	P 21/n	C 2/c	P -1
Hall group	-P 2yn	-C 2yc	-P 1
Crystal size (mm ³)	0.290 × 0.080 × 0.030	0.050 × 0.030 × 0.020	0.020 × 0.020 × 0.020
<i>a</i> [Å]	10.7047(16)	26.307(5)	13.649(3)
<i>b</i> [Å]	31.696(5)	13.465(3)	16.974(3)
<i>c</i> [Å]	14.247(2)	24.191(5)	18.357(4)
<i>α</i> [°]	90	90.00	85.19
<i>β</i> [°]	96.417	113.89	74.70
<i>γ</i> [°]	90	90	75.44
<i>V</i> [Å ³]	4803.7(12)	7835(3)	3969.9(16)
<i>Z</i>	4	8	2
ρ_{calc} [g/cm ³]	1.683	1.714	1.816
μ (Mo K α) [mm ⁻¹]	3.098	2.558	2.625
<i>h</i> , <i>k</i> , <i>l</i> max	15, 45, 20	41, 21, 38	18, 22, 24
Total reflections	14825	15804	18603
Unique reflections	13269	14301	15245
<i>R</i> _F , <i>R</i> _w (<i>F</i> ²) [<i>I</i> > 2 σ (<i>I</i>)]	0.0410, 0.0725	0.0316, 0.0799	0.0483, 0.0959
GOF on <i>F</i> ²	1.095	1.113	1.059
CCDC	1892788	1890707	1890708

Table S5. Selected bond distances, bond angles and dihedral angles from the optimized ground (S_0) and triplet state (T_1) geometry for the complexes **Ir1-Ir4** together with the experimental values.

	Ir1			Ir2			Ir3			Ir4		
	S_0	T_1	Exp									
Bond length (Å)												
Ir-C1	1.98921	1.98089	1.979	1.98955	1.98132	1.993	1.98951	1.97594	2.009	1.98841	1.97937	2.011
Ir-N1	2.08058	2.07627	2.074	2.08024	2.07519	2.102	2.07783	2.08212	2.099	2.07631	2.07178	2.088
Ir-C5	2.00120	1.96966	1.996	2.00233	1.96927	2.006	2.00036	1.97450	1.983	1.99871	1.96824	1.979
Ir-N2	2.08699	2.07022	2.093	2.08572	2.06925	2.091	2.08188	2.07959	2.064	2.08211	2.06695	2.082
Ir-N3	2.14624	2.16554	2.153	2.14546	2.16636	2.147	2.15025	2.15547	2.146	2.15201	2.17178	2.154
Ir-O1	2.14805	2.13947	2.148	2.14968	2.13922	2.156	2.14628	2.13813	2.154	2.14237	2.13137	2.149
Bond angle(deg)												
N1-Ir-C1	80.201	81.241	79.86	80.128	81.131	80.06	80.276	81.192	80.30	80.303	81.210	80.41
N2-Ir-C5	80.269	81.294	79.84	80.185	81.212	79.80	80.323	81.380	79.96	80.335	81.262	80.56
N3-Ir-O1	76.672	76.497	76.00	76.660	76.480	76.62	76.616	76.684	76.51	76.655	76.548	76.32
N1-Ir-N2	177.296	177.753	177.52	177.370	177.781	176.66	177.441	177.658	174.96	177.300	177.588	175.23
C5-Ir-N3	167.715	169.500	168.73	167.952	169.631	168.12	167.545	168.231	95.75	167.384	168.769	96.32
C1-Ir-O1	174.036	174.128	173.21	174.130	174.079	172.13	174.020	173.940	92.80	174.025	174.178	92.98
Interligand Angle (deg)												
N1-Ir-N3	83.878	82.340	82.15	83.859	82.321	99.99	83.761	82.547	98.68	83.753	82.286	99.11
N1-Ir-C5	97.498	98.172	97.71	97.691	98.312	99.43	97.683	97.920	101.54	97.556	98.328	98.77
Dihedral Angle (deg)												
C1-C2-C3-C4	177.463	179.831	177.26	178.917	178.449	174.74	178.387	179.472	174.35	177.939	179.271	177.90
C5-C6-C7-C8	177.657	177.325	172.22	175.970	175.712	179.46	177.166	176.783	177.17	177.868	177.241	177.37

Table S6. Optimized geometries, HOMO-2, HOMO-1, HOMO, LUMO, LUMO+1 and LUMO+2 contour plots of **Ir1-Ir4** at the PBE1PBE/6-31G* level.

	HOMO-2	HOMO-1	HOMO	Optimized structure	LUMO	LUMO+1	LUMO+2
Ir1							
Ir2							

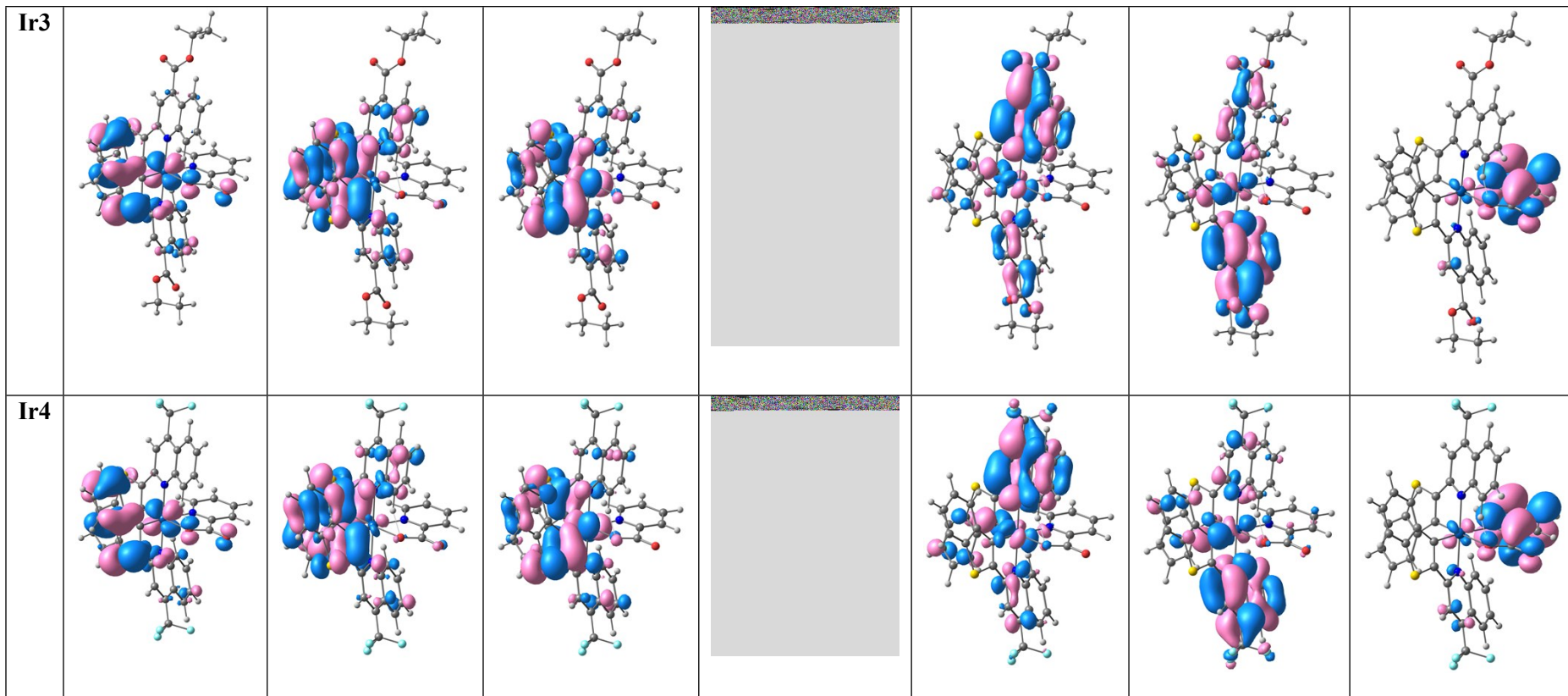


Table S7 Calculated energy levels of the HOMO, HOMO-1, HOMO-2, LUMO, LUMO+1, and LUMO+2 and percentage of contribution of iridium metal (Ir), benzothioquinolate derivatives and picolinate (pic) ligands.

Complex	Orbital	E (eV)	Iridium	Substituted Quinolate moiety	Benzothiophene moiety	Ancillary (pic)
Ir1	HOMO-3	-5.95	14.86	21.95	52.19	11
	HOMO-2	-5.824	31.23	13.99	43.91	10.87
	HOMO-1	-5.451	3.29	24.47	68.52	3.72
	HOMO	-4.904	26.14	17.79	53.75	2.32
	LUMO	-2.039	7.08	64.9	21.57	6.45
	LUMO+1	-2	4.39	66.88	19.76	8.97
	LUMO+2	-1.655	4.26	11.24	1.81	82.69
	LUMO+3	-1.199	1.03	30.79	7.61	60.58
Ir2	HOMO-3	-5.868	12.19	27.72	53.25	6.84
	HOMO-2	-5.736	34.69	20.44	33.49	11.37
	HOMO-1	-5.385	3.44	25.6	67.41	3.54
	HOMO	-4.836	26.29	17.83	53.53	2.35
	LUMO	-2.035	6.73	70.65	18.41	4.21
	LUMO+1	-1.981	4.15	71.22	16.69	7.94
	LUMO+2	-1.61	4.05	10.07	1.2	84.69
	LUMO+3	-1.165	0.97	36.38	11.72	50.94
Ir3	HOMO-3	-6.033	14.29	24.05	50.89	10.77
	HOMO-2	-5.926	23.26	13.81	55.04	7.88
	HOMO-1	-5.525	2.74	24.56	69.09	3.6
	HOMO	-5.003	25.07	18.78	53.97	2.18
	LUMO	-2.553	6.3	79.59	11.5	2.61
	LUMO+1	-2.492	5.37	81.82	10.28	2.53
	LUMO+2	-1.758	3.32	6.07	1.08	89.52
	LUMO+3	-1.364	1.42	43.4	27.16	28.03
Ir4	HOMO-3	-6.267	16.81	21.03	48.56	13.6
	HOMO-2	-6.142	19.91	11.73	61.76	6.6
	HOMO-1	-5.76	3.07	23.61	69.53	3.78
	HOMO	-5.241	24.55	18.76	54.61	2.09

	LUMO	-2.59	7.32	72.75	16.54	3.38
	LUMO+1	-2.532	5.35	75.13	15.43	4.1
	LUMO+2	-1.942	3.58	7.11	0.85	88.46
	LUMO+3	-1.551	1.01	49.91	20.75	28.33

Table S8 Calculated Absorption of **Ir1-Ir4** in CH₂Cl₂ Media at TD-B3LYP Level together with Experimental Values.

	State	$\lambda(\text{nm})/E(\text{eV})$	Oscillator	Main configuration	Assign	λ_{exp} (nm)
Ir1	S ₁ (triplet)	659/1.88	f=0.00001	H→L (58%)	btp/ Ir → Qn (ILCT/ MLCT)	634
	S ₂ (triplet)	650/1.90	f=0.00001	H→L+1 (57%)	btp/ Ir → Qn (ILCT/ MLCT/ LLCT)	
	S ₃ (singlet)	524/2.36	f=0.0284	H→L (70%)	btp/ Ir → Qn (ILCT/ MLCT)	530
	S ₄ (singlet)	520/2.38	f=0.1351	H→L+1 (69%)	btp/ Ir → Qn (ILCT/ MLCT/ LLCT)	
	S ₈ (singlet)	456/2.71	f=0.0099	H→L+2 (69%)	btp/ Ir → Qn/pic (ILCT/ MLCT/ LLCT)	
	S ₁₁ (singlet)	417/2.96	f=0.1470	H-1→L (67%)	btp → Qn (ILCT/ LLCT)	420
	S ₁₂ (singlet)	414/2.99	f=0.0673	H-1→L+1 (68%)	btp → Qn (ILCT/ LLCT)	
	S ₁₆ (singlet)	387/ 3.19	f=0.0605	H-2→L (59%)	btp/ Ir → Qn (ILCT/ MLCT)	
	S ₁₇ (singlet)	380/ 3.26	f=0.0063	H-2→L+1 (53%)	btp/ Ir → Qn (ILCT/ MLCT/ LLCT)	
	S ₁₈ (singlet)	378/3.28	f=0.0314	H→L+3 (64%)	btp/ Ir → Qn/pic (ILCT/ MLCT/ LLCT)	380
	S ₁₉ (singlet)	371/3.34	f=0.0077	H-1→L+2 (65%)	btp→ Qn/pic (ILCT / LLCT)	
	S ₂₀ (singlet)	367/3.37	f=0.0179	H-3→L (39%)	btp/ Ir → Qn (ILCT/ MLCT/ LLCT)	
Ir2	S ₁ (triplet)	664/1.87	f=0.0000	H→L (57%)	btp/ Ir → C ₆ H ₅ Qn (ILCT/ MLCT/ LLCT)	
	S ₂ (triplet)	655/1.89	f=0.0000	H→L+1 (56%)	btp/ Ir → C ₆ H ₅ Qn (ILCT/ MLCT/ LLCT)	637
	S ₃ (singlet)	534/2.32	f=0.0202	H→L (70%)	btp/ Ir → C ₆ H ₅ Qn (ILCT/ MLCT/ LLCT)	536
	S ₄ (singlet)	530/2.34	f=0.1771	H→L+1 (70%)	btp/ Ir → C ₆ H ₅ Qn (ILCT/ MLCT/ LLCT)	
	S ₈ (singlet)	458/2.71	f=0.0080	H→L+2 (70%)	btp/ Ir → pic (MLCT/ LLCT)	
	S ₁₁ (singlet)	425/2.92	f=0.1221	H-1→L (67%)	btp → C ₆ H ₅ Qn (ILCT/LLCT)	
	S ₁₂ (singlet)	420/2.95	f=0.0569	H-1→L+1 (68%)	btp → C ₆ H ₅ Qn (ILCT/LLCT)	
	S ₁₆ (singlet)	396/3.13	f=0.1802	H-2→L (65%)	btp/ Ir → C ₆ H ₅ Qn (ILCT/MLCT)	396
	S ₁₇ (singlet)	387/3.20	f=0.0133	H-2→L+1 (59%)	btp/ Ir → C ₆ H ₅ Qn (ILCT/MLCT)	
	S ₁₈ (singlet)	382/3.25	f=0.0243	H→L+3 (63%)	btp/ Ir → pic (MLCT/ LLCT)	
	S ₁₉ (singlet)	376/3.30	f=0.0187	H-3→L (66%)	btp/ Ir → C ₆ H ₅ Qn (ILCT/ MLCT)	
	S ₂₀ (singlet)	372/3.33	f=0.0143	H-1→L+2 (60%)	btp → pic (LLCT)	364
Ir3	S ₁ (triplet)	787/1.57	f=0.0000	H→L (61%)	btp/ Ir → COOEtQn (ILCT/ MLCT/ LLCT)	710
	S ₂ (triplet)	765/1.61	f=0.0000	H→L+1 (59%)	btp/ Ir → COOEtQn (ILCT/ MLCT/ LLCT)	
	S ₃ (singlet)	628/1.97	f=0.0259	H→L (70%)	btp/ Ir → COOEtQn (ILCT/ MLCT/ LLCT)	623
	S ₄ (singlet)	620/1.99	f=0.1059	H→L+1 (70%)	btp/ Ir → COOEtQn (ILCT/ MLCT/ LLCT)	570
	S ₉ (singlet)	488/2.53	f=0.0908	H-1→L (70%)	btp → COOEtQn (ILCT / LLCT)	490

	S ₁₀ (singlet)	482/2.57	f=0.0353	H-1→L+1 (70%)	btp → COOEtQn (ILCT / LLCT)	
	S ₁₃ (singlet)	452/2.74	f=0.0026	H→L+2 (70%)	btp/ Ir → pic (ILCT/ MLCT/ LLCT)	
	S ₁₅ (singlet)	433/2.85	f=0.1020	H-2→L (64%)	btp/ Ir → COOEtQn (ILCT/ MLCT/ LLCT)	420
	S ₁₇ (singlet)	419/2.95	f=0.0112	H-2→L+1 (59%)	btp/ Ir → COOEtQn (ILCT/ MLCT/ LLCT)	
	S ₁₈ (singlet)	409/3.02	f=0.0417	H-3→L (62%)	btp/ Ir → COOEtQn (ILCT/ MLCT/ LLCT)	
	S ₁₉ (singlet)	403/3.07	f=0.0835	H-3→L+1 (61%)	btp/ Ir → COOEtQn (ILCT/ MLCT/ LLCT)	
	S ₂₀ (singlet)	397/3.11	f=0.0659	H-4→L (53%)	btp/ Ir → COOEtQn (ILCT/ MLCT/ LLCT)	398
Ir4	S ₁ (triplet)	735/1.68	f=0.00001	H→L (56%)	btp/ Ir → CF ₃ Qn (ILCT/ MLCT/ LLCT)	688
	S ₂ (triplet)	722/1.71	f=0.00001	H→L (68%)	btp/ Ir → CF ₃ Qn (ILCT/ MLCT/ LLCT)	
	S ₄ (singlet)	574/2.15	f=0.1223	H→L+1 (68%)	btp/ Ir → CF ₃ Qn (ILCT/ MLCT/ LLCT)	575
	S ₉ (triplet)	458/2.70	f=0.1127	H-1→L (66%)	btp → CF ₃ Qn (ILCT)	468
	S ₁₀ (triplet)	453/2.73	f=0.0530	H-1→L+1 (67%)	btp → CF ₃ Qn (ILCT)	
	S ₁₂ (singlet)	444/2.78	f=0.0029	H→L+2 (69%)	btp/ Ir → pic (ILCT/ MLCT/ LLCT)	
	S ₁₆ (singlet)	412/3.00	f=0.0526	H-2→L (62%)	btp/ Ir → CF ₃ Qn (ILCT/ MLCT)	
	S ₁₇ (singlet)	401/3.09	f=0.0152	H-2→L+1 (58%)	btp/ Ir → CF ₃ Qn (ILCT/ MLCT)	
	S ₁₈ (singlet)	390/3.17	f=0.0400	H-3→L (52%)	btp/ pic/ Ir → CF ₃ Qn (ILCT/ MLCT/ LLCT)	
	S ₁₉ (singlet)	385/3.21	f=0.0629	H-3→L+1 (45%)	btp/ pic/ Ir → CF ₃ Qn (ILCT/ MLCT/ LLCT)	
	S ₂₀ (singlet)	382/3.24	f=0.0948	H-3→L+1 (35%)	btp/ pic/ Ir → CF ₃ Qn (ILCT/ MLCT/ LLCT)	401
	S ₂₀ (singlet)	391/3.16	f=0.0442	H-3→L (53%)	btp/ Ir → CF ₃ Qn (ILCT/ MLCT/ LLCT)	

REFERENCES

1. F. O. Garces, K. A. King and R. J. Watts, *Inorg. Chem.*, 1988, **27**, 3464-3471.
2. Hae Un Kim, Sunyoung Sohn, Wanuk Choi, Minjun Kim, Seung Un Ryu, Taiho Park, Sungjune Jung, K. S. Bejoymohandas, *J. Mater. Chem. C*, 2018, **6**, 10640
3. Y. Liu, M. S. Liu and A. K. Y. Jen, *Acta Polym.*, 1999, **50**, 105-108.
4. S. I. Gorelsky, *SWizard program (version 4.6)*, 2007.
5. M. J. Frisch, G. W. Trucks, H. B. Schlegel, G. E. Scuseria, M. A. Robb, J. R. Cheeseman, G. Scalmani, V. Barone, G. A. Petersson, H. Nakatsuji, X. Li, M. Caricato, A. V. Marenich, J. Bloino, B. G. Janesko, R. Gomperts, B. Mennucci, H. P. Hratchian, J. V. Ortiz, A. F. Izmaylov, J. L. Sonnenberg, Williams, F. Ding, F. Lipparini, F. Egidi, J. Goings, B. Peng, A. Petrone, T. Henderson, D. Ranasinghe, V. G. Zakrzewski, J. Gao, N. Rega, G. Zheng, W. Liang, M. Hada, M. Ehara, K. Toyota, R. Fukuda, J. Hasegawa, M. Ishida, T. Nakajima, Y. Honda, O. Kitao, H. Nakai, T. Vreven, K. Throssell, J. A. Montgomery Jr., J. E. Peralta, F. Ogliaro, M. J. Bearpark, J. J. Heyd, E. N. Brothers, K. N. Kudin, V. N. Staroverov, T. A. Keith, R. Kobayashi, J. Normand, K. Raghavachari, A. P. Rendell, J. C. Burant, S. S. Iyengar, J. Tomasi, M. Cossi, J. M. Millam, M. Klene, C. Adamo, R. Cammi, J. W. Ochterski, R. L. Martin, K. Morokuma, O. Farkas, J. B. Foresman and D. J. Fox, *Gaussian 16 Rev. B.01*, Wallingford, CT, 2016.